Human lungs show limited permissiveness for SARS-CoV-2 due to scarce ACE2 levels but virus-induced expansion of inflammatory macrophages

Katja Hönzke[1,20], Benedikt Obermayer[2,20], Christin Mache[3,20], Diana Fathykova[1], Mirjana Kessler[1,4], Simon Dökel[5], Emanuel Wyler[6], Morris Baumgardt[1], Anna Löwa[1], Karen Hoffmann[1], Patrick Graff[1], Jessica Schulze[3], Maren Mieth[1], Katharina Hellwig[1], Zeynep Demir[1], Barbara Biere[3], Linda Brunotte[7], Angeles Mecate-Zambrano[7], Judith Bushe[5], Melanie Dohmen[1,8], Christian Hinze[8,9], Sefer Elezkurtaj[10], Mario Tönnies[11], Torsten T. Bauer[11], Stephan Eggeling[12], Hong-Linh Tran[12], Paul Schneider[13], Jens Neudecker[14], Jens C. Rückert[14], Kai M. Schmidt-Ott[8,9], Jonas Busch[15], Frederick Klauschen[10], David Horst[10], Helena Radbruch[16], Josefine Radke[16], Frank Heppner[16], Victor M. Corman[17], Daniela Niemeyer[17], Marcel A. Müller[17], Christine Goffinet[17], Ronja Mothes[18,19], Anna Pascual-Reguant[18,19], Anja Erika Hauser[18,19], Dieter Beule[2], Markus Landthaler[6], Stephan Ludwig[7], Norbert Suttorp[1], Martin Witzenrath[1], Achim D. Gruber[5], Christian Drosten[17], Leif-Erik Sander[1], Thorsten Wolff[3], Stefan Hippenstiel[1] and Andreas C. Hocke[1]

[1]Department of Infectious Diseases and Respiratory Medicine, Charité – Universitätsmedizin Berlin, corporate member of Freie Universität Berlin, Humboldt-Universität zu Berlin, Berlin, Germany. [2]Berlin Institute of Health at Charité – Universitätsmedizin Berlin, Core Unit Bioinformatics, Berlin, Germany. [3]Unit 17 "Influenza and other Respiratory Viruses", Robert Koch Institut, Berlin, Germany. [4]Department of Gynecology and Obstetrics, Ludwig-Maximilian University, Munich, Germany. [5]Department of Veterinary Pathology, Freie Universität Berlin, Berlin, Germany. [6]Berlin Institute for Medical Systems Biology (BIMSB), Max Delbrück Center for Molecular Medicine in the Helmholtz Association (MDC) and IRI Life Sciences, Institute for Biology, Humboldt Universität zu Berlin, Berlin, Germany. [7]Institute of Virology, Westfaelische Wilhelms Universität, Münster, Germany. [8]Max Delbrück Center for Molecular Medicine in the Helmholtz Association, Berlin, Germany. [9]Department of Nephrology and Medical Intensive Care, Charité – Universitätsmedizin Berlin, corporate member of Freie Universität Berlin, Humboldt-Universität zu Berlin, Berlin, Germany. [10]Department of Pathology, Charité – Universitätsmedizin Berlin, corporate member of Freie Universität Berlin, Humboldt-Universität zu Berlin, Berlin, Germany. [11]HELIOS Clinic Emil von Behring, Department of Pneumology and Department of Thoracic Surgery, Chest Hospital Heckeshorn, Berlin, Germany. [12]Department of Thoracic Surgery, Vivantes Clinics Neukölln, Berlin, Germany. [13]Department for Thoracic Surgery, DRK Clinics, Berlin, Germany. [14]Department of General, Visceral, Vascular and Thoracic Surgery, Charité – Universitätsmedizin Berlin, corporate member of Freie Universität Berlin, Humboldt-Universität zu Berlin, Berlin, Germany. [15]Clinic for Urology, Charité – Universitätsmedizin Berlin, corporate member of Freie Universität Berlin, Humboldt-Universität zu Berlin, Berlin, Germany. [16]Institute for Neuropathology, Charité – Universitätsmedizin Berlin, corporate member of Freie Universität Berlin, Humboldt-Universität zu Berlin, Berlin, Germany. [17]Institute of Virology, Charité – Universitätsmedizin Berlin, corporate member of Freie Universität Berlin, Humboldt-Universität zu Berlin, Berlin, Germany. [18]Department of Rheumatology and Clinical Immunology, Charité – Universitätsmedizin Berlin, corporate member of Freie Universität Berlin and Humboldt-Universität zu Berlin, Berlin, Germany. [19]Deutsches Rheuma-Forschungszentrum (DRFZ), a Leibniz Institute, Berlin, Germany. [20]Contributed equally.

Corresponding author: Andreas C. Hocke (andreas.hocke@charite.de)

Shareable abstract (@ERSpublications)
Scarce ACE2 expression limits alveolar permissiveness for SARS-CoV-2. Viral uptake by alveolar macrophages leads to a specific immune activation. COVID-19 ARDS is likely caused by secondary immunopathogenesis rather than direct alveolar viral damage. https://bit.ly/3ar4ei5

Cite this article as: Hönzke K, Obermayer B, Mache C, *et al*. Human lungs show limited permissiveness for SARS-CoV-2 due to scarce ACE2 levels but virus-induced expansion of inflammatory macrophages. *Eur Respir J* 2022; 60: 2102725 [DOI: 10.1183/13993003.02725-2021].

Abstract

Background Severe acute respiratory syndrome coronavirus 2 (SARS-CoV-2) utilises the angiotensin-converting enzyme 2 (ACE2) transmembrane peptidase as cellular entry receptor. However, whether

This article has an editorial commentary: https://doi.org/10.1183/13993003.01521-2022

Received: 15 Oct 2021
Accepted: 25 May 2022

SARS-CoV-2 in the alveolar compartment is strictly ACE2-dependent and to what extent virus-induced tissue damage and/or direct immune activation determines early pathogenesis is still elusive.

Methods Spectral microscopy, single-cell/-nucleus RNA sequencing or ACE2 "gain-of-function" experiments were applied to infected human lung explants and adult stem cell derived human lung organoids to correlate ACE2 and related host factors with SARS-CoV-2 tropism, propagation, virulence and immune activation compared to SARS-CoV, influenza and Middle East respiratory syndrome coronavirus (MERS-CoV). Coronavirus disease 2019 (COVID-19) autopsy material was used to validate *ex vivo* results.

Results We provide evidence that alveolar ACE2 expression must be considered scarce, thereby limiting SARS-CoV-2 propagation and virus-induced tissue damage in the human alveolus. Instead, *ex vivo* infected human lungs and COVID-19 autopsy samples showed that alveolar macrophages were frequently positive for SARS-CoV-2. Single-cell/-nucleus transcriptomics further revealed nonproductive virus uptake and a related inflammatory and anti-viral activation, especially in "inflammatory alveolar macrophages", comparable to those induced by SARS-CoV and MERS-CoV, but different from NL63 or influenza virus infection.

Conclusions Collectively, our findings indicate that severe lung injury in COVID-19 probably results from a macrophage-triggered immune activation rather than direct viral damage of the alveolar compartment.

Introduction

Coronavirus disease 2019 (COVID-19) is caused by the severe acute respiratory syndrome coronavirus 2 (SARS-CoV-2). Depending on the virus variant, ~22% of COVID-19 patients develop severe disease with a high risk of acute respiratory distress syndrome (ARDS) [1–5], which may be heterogeneous and differ from classical ARDS [6]. Both SARS-CoV-2 and SARS-CoV use angiotensin-converting enzyme 2 (ACE2) as primary cellular entry receptor [7, 8]. However, to what extent ACE2 contributes to alveolar pathogenesis which may result in subsequent lung failure remains elusive. Thus, the actual role of ACE2 in COVID-19 pathogenesis is still a matter of debate [9–11]. While some studies suggested relatively high or induced ACE2 expression under healthy or pulmonary diseased conditions [12–18], others suggest relatively low, cell type-limited ACE2 expression in the alveolus [11, 14, 19–21]. This is complicated by the fact that some of these studies solely focus on *ACE2* mRNA analyses which might differ from the actual ACE2 protein expression level [11, 20, 22–24]. Consequently, to gain deeper insight into COVID-19 pathogenesis, further rigorous analyses of tissue- and cell type-specific ACE2 mRNA and protein expression in the context of SARS-CoV-2 tropism, replication and resulting tissue damage and/or induced immune response in the early phase of infection are required.

Similarly, there is still inconsistency about the actual SARS-CoV-2 tropism as well as replication efficacy in the human alveolar compartment and a debate if and to what extent alveolar epithelial type 1 (AT1), type 2 cells (AT2) or alveolar macrophages become productively infected and contribute to tissue pathology [20, 25–27]. Although it appears obvious that alveolar ACE2 is present and viral infection of alveolar cells occurs, it is critical to elucidate the role of direct infection *versus* indirect immunopathology in the pathogenesis of COVID-19 ARDS. Of note, some clinical trials have demonstrated beneficial effects of dexamethasone in severe COVID-19, suggesting immune-related instead of direct viral replication-associated lung damage [28–30].

Therefore, we aimed to elucidate ACE2 dependency for alveolar SARS-CoV-2 tropism, productive infection, replication rate, tissue damage and immune activation across cells of the alveolar space. By several independent methods using *ex vivo* infected human lung tissue, COVID-19 autopsy material and adult stem cell derived human lung organoids, we demonstrate scarce ACE2 mRNA and protein expression restricted to AT2 cells without statistically significant induction of ACE2 protein by interferon (IFN). Accordingly, SARS-CoV and SARS-CoV-2 propagated consistently less efficient compared to influenza (IAV) and Middle East respiratory syndrome coronavirus (MERS-CoV) in human lung tissue. ACE2 overexpression in human lungs broadens SARS-CoV-2 tropism as well as tissue damage, similar to MERS-CoV. SARS-CoV-2 is predominantly endocytosed by alveolar macrophages leading to an expansion of inflammatory alveolar macrophages in human lung explants and COVID-19 autopsy lungs, resulting in a coronavirus-specific inflammatory and antiviral gene expression signature.

Methods

Detailed information is outlined in the supplementary material.

Models used

For *ex vivo* infection of human lung tissue samples, fresh lung explants were obtained from 25 patients suffering from lung carcinoma (one case metastatic osteosarcoma), who underwent lung resection at local

thoracic surgeries. Lung explants from healthy patients were obtained from the International Institute for the Advancement of Medicine (Edison, NJ, USA). Clinical data of donors are included in supplementary table S1 (ethics approval Charité EA2/079/13 and Ärztekammer Westfalen-Lippe AZ: 2016-265-f-S). Primary alveolar macrophages were isolated by repeated perfusion of the human explant lungs. For the alveolar and bronchial organoids, primary cells were isolated from noncancerous (normal) parts of distal lung tissue obtained from lung cancer patients undergoing tumour resection surgery. Kidney tissue was collected from tumour nephrectomies (ethics approval EA4/026/18). Autopsy material was included from 25 cases of patients who had died after COVID-19 disease. Autopsies were performed on the legal basis of §1 SRegG BE of the autopsy act of Berlin and §25(4) of the German Infection Protection Act. This study was approved by the ethics committee of the Charité (EA 1/144/13 and EA2/066/20) as well as by the Charité-BIH COVID-19 research board and was in compliance with the Declaration of Helsinki.

Virus strains

Infection experiments were carried out by two independent laboratories in Berlin (Robert Koch Institute and Charité) and Muenster (Wilhelms-University in Muenster). For infection experiments, SARS-CoV-2 (Munich 929 or BavPart1) [7], rSARS-CoV (generated in the Drosten Lab by reverse genetics based on the SARS-CoV Frankfurt-1 strain, accession number FJ429166.1 [31]), SARS-CoV-2 FI-200 isolate strain, rMERS-CoV (generated in the Drosten Lab by reverse genetics based on the MERS-CoV strain EMC/2012, accession number JX869059 [32]), HCoV-NL63 and the human seasonal influenza H3N2 virus A/Panama/2007/1999 (Pan/99[H3N2]) (further referred to as IAV) strains were used.

Infection experiments and infectious particle quantification

Calu-3 cells were either mock-infected with infection medium or challenged with SARS-CoV-2, rSARS-CoV, rMERS-CoV or IAV (multiplicity of infection (MOI) 0.1). Lung tissue cultures were inoculated with control medium or SARS-CoV-2, rSARS-CoV, rMERS-CoV or IAV.

Samples

Mature human lung organoids were collected, broken up and organoid fragments were either mock-infected or challenged with SARS-CoV-2. Alveolar macrophages were infected with control medium, SARS-CoV-2 or hCoV-NL63. Samples were taken at the indicated time points.

IFN stimulation of lung tissue

Culture medium containing recombinant human IFNβ (100 $U \cdot mL^{-1}$) was injected into lung explants. The tissue was processed for RNA and protein analysis after an additional 24 h or 96 h.

Bulk RNA sequencing and analysis

RNA from infected samples was purified. $PolyA^+$ RNA sequencing libraries were constructed using the NEBNext Ultra II Directional RNA Library Prep Kit for Illumina (New England Biolabs) according to the manufacturer's instructions and sequenced on a Nextseq 500 device using 1×76 cycles single-end sequencing.

Single-cell isolation and library preparation

Single cells from individual human lung tissue samples were isolated. Alveolar macrophages were detached using a cell scraper. The single-cell capturing and downstream library constructions were performed using the Chromium Single Cell 3′ V3.1 library preparation kit according to the manufacturer's protocol (10x Genomics). The constructed libraries were either sequenced on the Nextseq 500 using 28 cycles for read 1, 55 cycles for read 2 and eight index cycles, or on the Novaseq 6000 S1 using 28 cycles for read 1, 64 cycles for read 2 and eight index cycles, to a median depth of 36 000 reads per cell.

Single-nucleus isolation and library preparation

Single nuclei were isolated from snap-frozen autopsy samples as described previously [33].

In situ *hybridisation*

For RNA *in situ* hybridisation (ISH), tissues were immersion-fixed and embedded in paraffin.

ISH for the detection of SARS-CoV-2 and MERS-CoV was performed using the ViewRNA ISH Tissue Assay (Invitrogen by Thermo Fisher Scientific) following the manufacturer's instructions (MAN0018633 Rev.C.0), as described previously [34].

Image segmentation

From each COVID-19 (n=4) and non-COVID-19 (n=4) haematoxylin and eosin-stained tissue slide, two regions of interest (15 000×15 000 and 20 000×20 000 pixel/19 360 000 μm^2 and 10 890 000 μm^2, in total 30.25 mm^2) were extracted and the number of cell nuclei was determined. Cell nuclei were separated from background by manual thresholding of hue and brightness channels in a hue, saturation, brightness representation of the coloured microscopy images. Cell nuclei were separated from each other by morphological filtering and distance transform watershed using the MorphoLibJ-Plugin [35] of Fiji [36].

Results

ACE2 is scarcely expressed in the human alveolar compartment

ACE2, transmembrane protease serine subtype 2 (TMPRSS2), furin and further host factors are considered as determinants of SARS-CoV-2 cellular entry and infection [7, 37]. To quantify their expression across alveolar space, we performed single-cell (scSeq) and single-nucleus RNA sequencing (snSeq) of human lung tissue samples (six donors) and control autopsy lungs (two donors) (figure 1a, supplementary tables S1 and S2) and annotated cell clusters (figure 1b, supplementary figure S1a and b, supplementary table S3) [38]. While *TMPRSS2* was highly expressed in AT1 and AT2 cells, only three out of 2199 AT2 cells were *ACE2* positive, expressing only one unique molecular identifier each (figure 1c) [18, 22, 23]. In contrast, the proposed alternative SARS-CoV-2 receptors *KREMEN1*, *ASGR1*, *CD147* (*BSG*) as well as *FURIN* were ubiquitously expressed in human lung explants and in autopsy lungs (figure 1c) [39–42]. We confirmed this trend for *ACE2*, *BSG*, *TMPRSS2* and *FURIN* by reverse transcriptase (RT) quantitative (q) PCR on bulk RNA of human lung tissue and human lung bronchial organoids as well as Calu-3 cells as positive control (figure 1d). For ACE2 protein analysis, we evaluated five commercial ACE2 antibodies on Calu-3 cells and found the R&D AF933 to be the most sensitive and specific, which was chosen for further experiments (supplementary figure S1c). Western blot analysis showed very high ACE2 protein amounts in kidneys [43], whereas levels in lung tissue and bronchial organoids were low or undetectable (figure 1e/long exposure, supplementary figure S1d/short exposure, supplementary table S1). Lung tissue explants obtained from cancer patients were referenced against "normal" lung tissue from transplant donors showing the same low ACE2 protein amounts (supplementary figure S1e).

Since *ACE2* has been identified as an IFN-stimulated gene (ISG) [18, 23], we stimulated lung tissue with IFNβ (figure 1f and g, supplementary table S1). Although RT-qPCR analysis showed ∼40-fold induction of *ACE2* after 96 h, no upregulation of ACE2 was detected at the protein level. Significant induction was observed for *BSG* and positive control gene *MX1*, but not for *TMPRSS2* or *FURIN* (figure 1f).

We performed immunostaining and *in situ* hybridisation for ACE2 and TMPRSS2 in lung tissue and bronchial organoids to evaluate cell type-specific expression patterns (figure 2 and supplementary figure S2). In alveoli, ACE2 protein and mRNA expression levels were rather low and nearly undetectable by conventional, threshold-based confocal microscopy (supplementary figure S2b). Using spectral imaging and linear unmixing, ACE2 protein and mRNA could be detected in few AT2 cells (∼5.6%) (figure 2a and supplementary figure S2b and d). AT2 cells positive for *ACE2* mRNA did not necessarily exhibit ACE2 surface protein expression. To further demonstrate the importance of antibody evaluation we tested another ACE2 antibody (Thermo PA5–20046) with available blocking peptide (supplementary figure S2c, insets). Immunostaining revealed a similar expression pattern to that demonstrated by Hamming *et al.* [12] with abolishment of the signal by blocking peptide pre-incubation. However, further validation by Western blot revealed an indefinite band pattern completely abolished by blocking peptide indicating abundant, but likely unspecific antibody binding and false-positive ACE2 expression in AT1 and AT2 cells in human lung tissue using this antibody. In line with scSeq, *TMPRSS2* was found frequently expressed in AT1 and AT2 cells, but was not detected in alveolar macrophages (figure 2b). Calu-3 cells and kidney served as positive control for *ACE2*, *TMPRSS2* and ACE2 protein expression (supplementary figure S2a).

Scarce ACE2 expression limits SARS-CoV-2 replication, tropism and tissue damage

In previous studies, we established *ex vivo* cultured human lung tissue as an infection model to assess the virulence of respiratory viruses such as IAV and MERS-CoV [44–46]. Replication of several IAV strains as well as MERS-CoV was observed in this model system, in line with alveolar expression of the corresponding receptors [45, 46]. Therefore, we infected lung tissue (five donors) with SARS-CoV-2 and compared its replication to IAV, MERS-CoV and SARS-CoV. We found highly variable and moderate replication for the ACE2-dependent SARS-CoV and SARS-CoV-2, whereas IAV and MERS-CoV replicated more efficiently (figure 3a, supplementary table S1). An external, independent validation experiment (three donors) showed a similar kinetic of SARS-CoV-2 in human lung tissue (supplementary figure S3a). We confirmed low replication (four donors) by increasing the infection dose of SARS-CoV-2 (30-fold) resulting in only a minor increase of SARS-CoV-2 followed by a rapid decline below input,

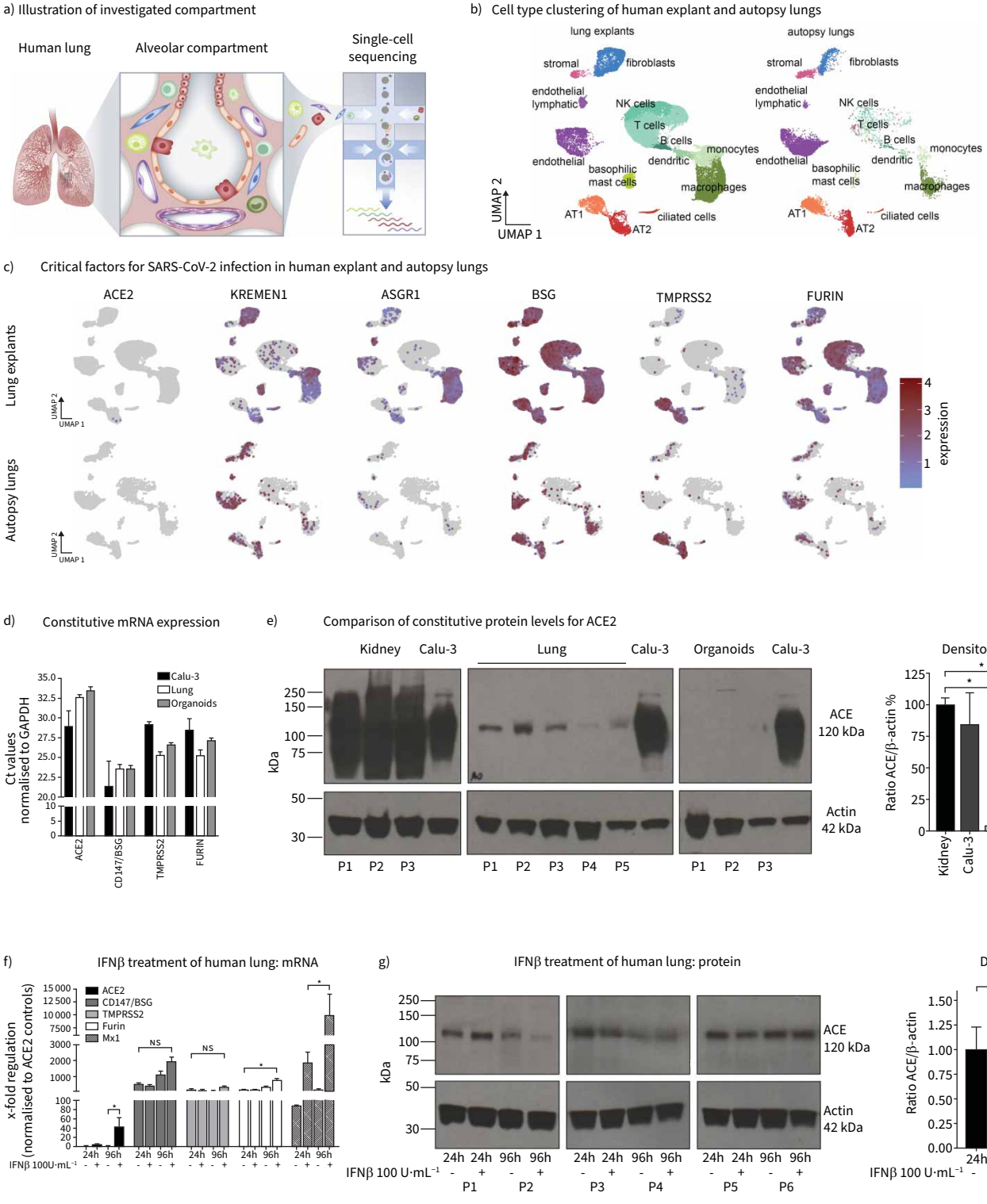

FIGURE 1 Angiotensin-converting enzyme 2 (ACE2) expression is scarce in human lungs and cannot be induced by interferon (IFN) at the protein level. a) Schematic illustration of cell types of the investigated alveolar compartment as well as single-cell RNA sequencing (scSeq). b) Annotation of cell clusters from scSeq and single-nucleus RNA sequencing (snSeq) of human lung tissue and autopsy material, respectively. Confirmation of major cell types by related marker gene expression is presented in supplementary figure S1a and b. c) Comparison of scarce *ACE2* expression in alveolar epithelial type 2 (AT2) cells with abundant *KREMEN1*, *ASGR1*, *CD147/BSG*, *TMPRSS2* and *FURIN* expression by scSeq and snSeq. d) Analysis of *ACE2*, *CD147/BSG*, *TMPRSS2* and *FURIN* expression by quantitative (q)PCR on bulk RNA of normal human lung tissue, human bronchial organoids and Calu-3 cells. Ct values are normalised to glyceraldehyde 3-phosphate dehydrogenase (GAPDH) expression to demonstrate absolute levels of ACE2 compared to other factors. e) Analysis of constitutive ACE2 expression by Western blot using the R&D AF933 antibody. Antibody evaluation is

presented in supplementary figure S1c. Shown are protein lysates from human kidneys (three donors), human lungs (five donors), human bronchial organoids (three donors) and Calu-3 cells. Prolonged exposure time (30 s) of membranes was carried out to demonstrate scarce ACE2 expression in lungs and bronchial organoids compared to kidneys and Calu-3. Exposure time of 1 s is shown in supplementary figure S1d. β-Actin served as loading control. Densitometric analysis shows semi-quantitative ACE2 expression normalised to β-actin (right panel). f) Human lung tissue was stimulated for 24 h and 96 h with IFNβ and *ACE2*, *CD147/BSG*, *TMPRSS2*, *FURIN* and *Mx1* expression was analysed by qPCR on bulk RNA. g) Western blot analysis of ACE2 expression in IFNβ-stimulated human lung tissue after 24 h and 96 h of six donors and corresponding densitometric analysis normalised to β-actin. Data are presented as mean±SEM. NK: natural killer; UMAP: Uniform Manifold Approximation and Projection. *: p<0.05.

whereas replication of other viruses was similar (figure 3b, supplementary table S1). Calu-3 cells served as a positive control (figure 3c).

In order to assess the role of low ACE2 expression in the limited permissiveness of lung tissue for SARS-CoV-2, we compared viral replication in wild-type and $ACE2^+$ human bronchial organoids. ACE2 overexpression led to comparable protein levels as shown for Calu-3 cells and apical ACE2 expression on a subpopulation of bronchial organoid cells (figure 3d and e). Although *ACE2* mRNA was detectable in almost all organoid cells, apical ACE2 protein was expressed only on a subpopulation of cells (figure 3e). SARS-CoV-2 S-protein was only observed in ACE2 protein positive bronchial organoid cells (figure 3e) and only $ACE2^+$ bronchial organoids supported SARS-CoV-2 replication (figure 3f). We substantiated the relevance of this finding to ACE2-dependent permissiveness of human lung tissue to SARS-CoV-2 by examining human alveolar organoids that support active replication of SARS-CoV-2 without ACE2 overexpression (figure 3g). We profiled ∼3000 and ∼23 000 cells from alveolar and bronchial organoids, respectively, and annotated and quantified the cell type composition (supplementary figure S3b, c and e). AT2-like cells with constitutive expression of ACE2 (mRNA scSeq and apical protein) were found exclusively in alveolar organoids (figure 3h and supplementary figure S3d–f). Other relevant host factors such as *KREMEN1*, *ASGR1*, *TMPRSS2*, *FURIN*, *BSG* and *NRP1* were equally well expressed in both organoid types (supplementary figure S3d). Correspondingly, SARS-CoV-2 RNA could be detected in many cells of alveolar, but not bronchial, organoids (figure 3h and supplementary figure S3e). This is in line with SARS-CoV-2 N-protein detection by immunostaining in ACE2-positive cells of alveolar organoids (figure 3i). However, ACE2 protein expression is detectable at very low levels in alveolar organoids, but not $ACE2^+$ bronchial organoids (supplementary figure S3f).

Immunostaining and *in situ* hybridisation was performed in human lung tissue explants to determine ACE2-dependent SARS-CoV-2 cellular tropism and tissue damage (figure 4). In line with low alveolar ACE2 expression, we rarely found SARS-CoV-2 infected AT2 cells by complementary methods (*N-gene*, *S-gene*, N-protein, S-protein labelling) (figure 4a and b), whereas MERS-CoV showed widespread infection (supplementary figure S4a) [45]. Instead of broad epithelial infection, we frequently detected punctuated staining in alveolar macrophages positive for SARS-CoV-2 (viral RNA, viral proteins) (figure 4a and b). Mock- and SARS-CoV-2-infected Calu-3 cells served as controls (supplementary figure S4b).

To show that SARS-CoV-2 tropism is limited by ACE2 expression, we overexpressed ACE2 ($ACE2^+$) by adenoviral transduction in the explant tissue and detected strong apical ACE2 expression in AT1 and AT2 cells, endothelial cells, bronchial epithelium and alveolar macrophages (figure 4c and supplementary figure S4c). The punctuated staining pattern for SARS-CoV-2 in $ACE2^+$ alveolar macrophages (figure 4b) changed to a cytosolic pattern comparable to AT2 cells and showed signs of alveolar macrophage apoptosis, indicating productive infection if ACE2 is present in these cell types (figure 4c). Next, we investigated whether broadened alveolar ACE2 expression and subsequent SARS-CoV-2 tropism might lead to increased tissue damage by using delinearisation and loss of epithelial occludin as surrogate [45]. In early infections (16–24 h) of wild-type and $ACE2^+$ lungs with SARS-CoV-2 and MERS-CoV, infected AT2 cells still showed a linear occludin pattern similar to mock infection (figure 4d and supplementary figure S4c). In late infection (72 h), the $ACE2^+$ induced a broadened SARS-CoV-2 tropism, increased detachment of infected cells and loss of epithelial occludin, similar to the strong damage pattern of MERS-CoV (figure 4d) [45].

Ex vivo infected tissue only partially reflects the pathophysiology of lungs in COVID-19 patients. Therefore, we investigated peripheral lung tissue of 25 confirmed COVID-19 autopsy cases by *in situ* hybridisation against *N-gene* of SARS-CoV-2 and found just two patients (one of them very moderately) positive for cellular SARS-CoV-2, although 18 out of 25 exhibited viral RNA in the lungs (RT-qPCR; figure 5 and supplementary figure S5) [47]. While 24 patients (P2–P25) underwent intensive care treatment

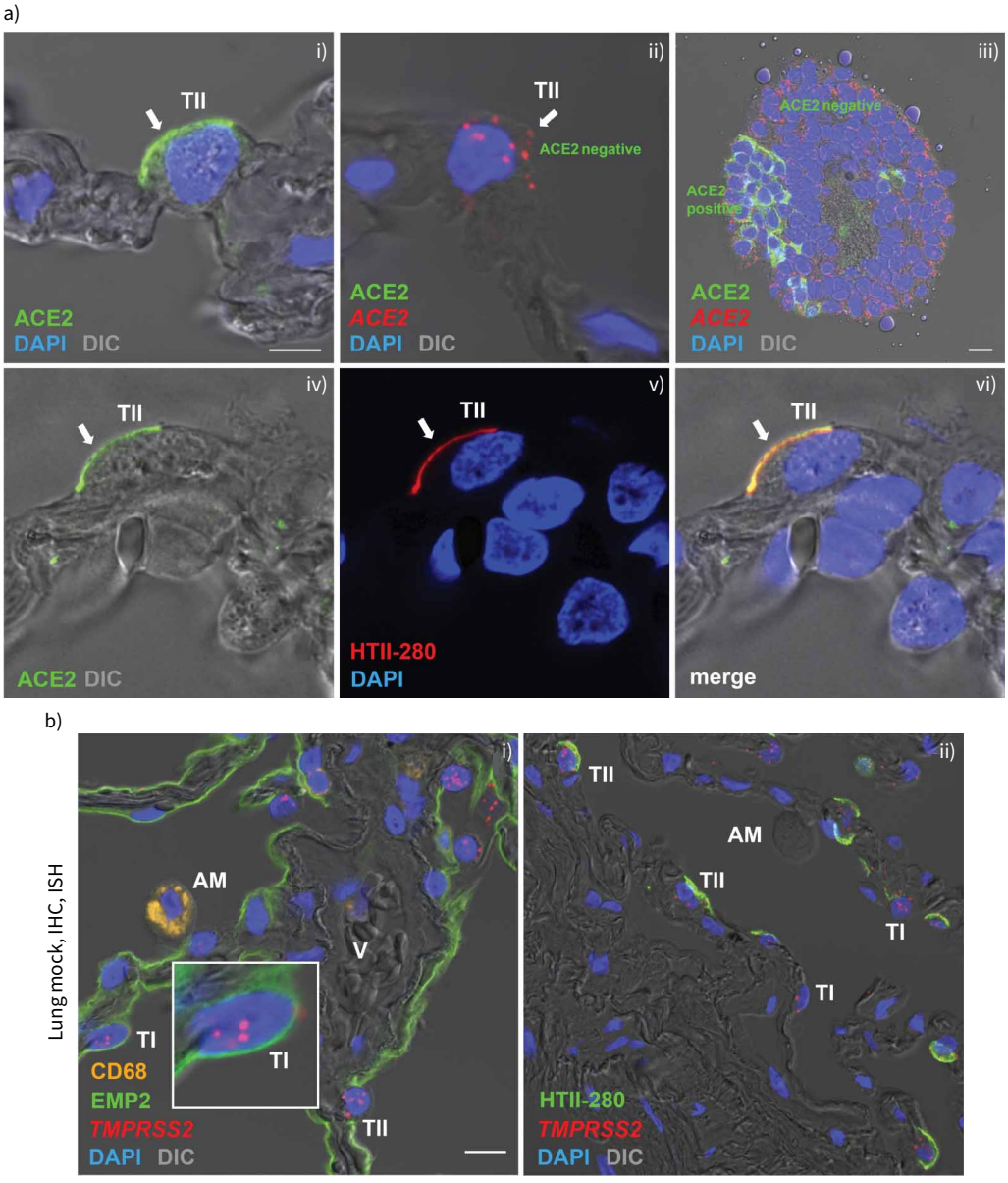

FIGURE 2 Spectral imaging reveals scarce apical angiotensin-converting enzyme 2 (ACE2) on alveolar epithelial type 2 (AT2) cells, less congruence with *ACE2* as well as abundant *TMPRSS2* expression in AT1 and AT2. Immunohistochemistry and *in situ* hybridisation were analysed in human lung tissue and organoids by spectral microscopy and linear unmixing. a) Panel i) shows single-channel detection (to avoid antibody cross-reactivity) of ACE2 immunostaining (green) on the apical surface of an AT2 cell (TII). AT2/ACE2 expression was confirmed by dual-channel detection with AT2 marker HTII-280 (red) in panels iv–vi) (arrows). Panel ii) shows *ACE2* mRNA (red) in an AT2 cell. Sequential immunostaining could not reveal ACE2 protein on the apical surface (arrow). Lack of apical ACE2 protein in a fraction of *ACE2* mRNA (red) positive cells is demonstrated by lentiviral overexpression in a human bronchial organoid in panel iii). Parts of the cells show apical ACE2 (green) as well. Cell nuclei are visualised by 4′,6-diamidino-2-phenylindole (DAPI) stain (blue). Scale bars: 5 µm (lungs), 10 µm (bronchial organoids). b) Immunostaining for CD68 (alveolar macrophages (AM), orange) and EMP2 (AT1, green) as well as *in situ* hybridisation for *TMPRSS2* (red, panel i)) and HTII-280 (AT2, panel ii), green) in human lung tissue shows *TMPRSS2* positive in AT1 (inset) and AT2, but not vessels (V) or AM. Cell nuclei are visualised by DAPI stain (blue). Scale bar: 10 µm. ACE2 expression in Calu-3 cells and kidneys as well as ACE2 antibody tests are presented in supplementary figure S2.

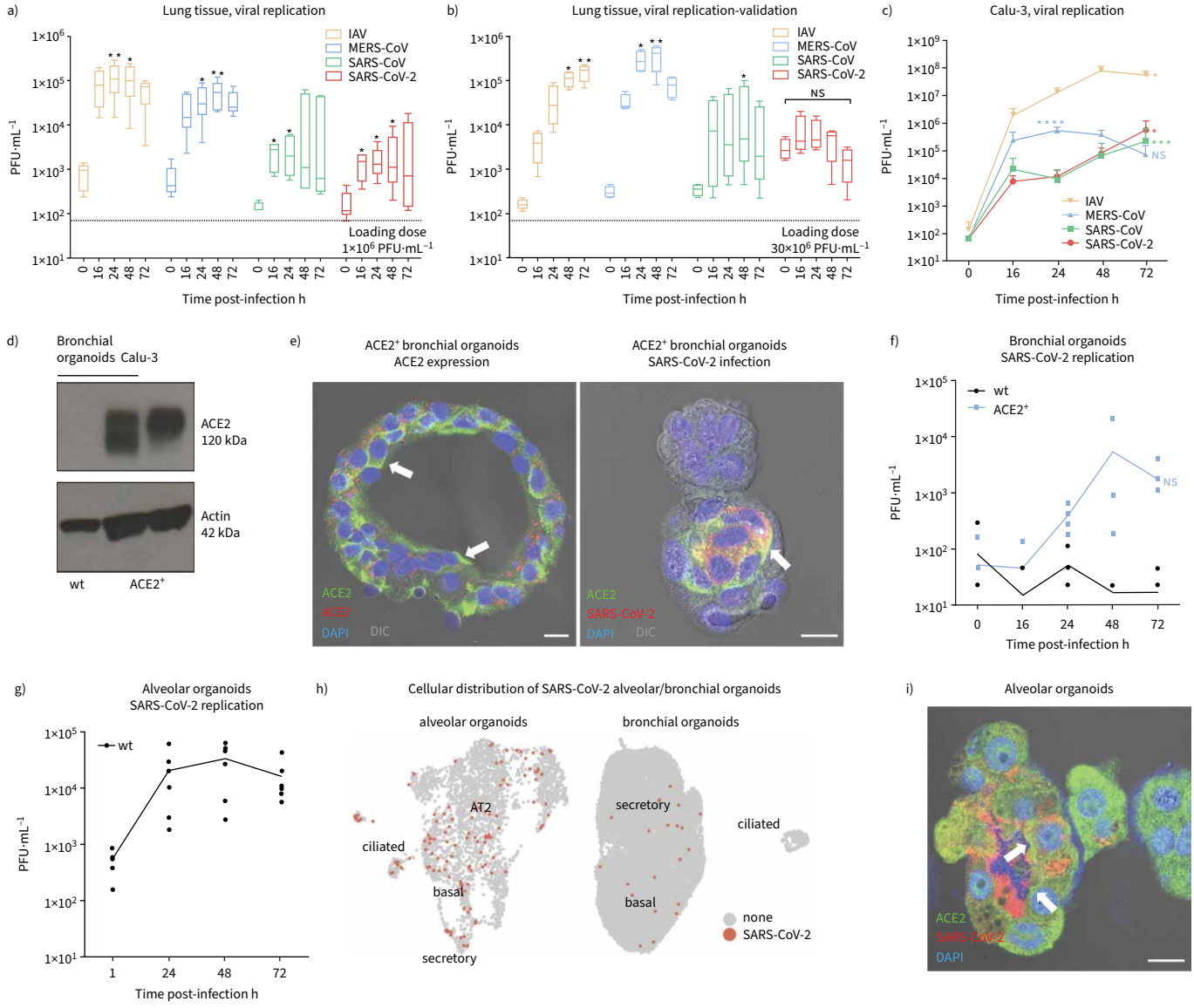

FIGURE 3 Severe acute respiratory syndrome coronavirus 2 (SARS-CoV-2) shows low replication on human lung tissue, which can be increased by angiotensin-converting enzyme 2 (ACE2) overexpression. a) Human lung tissue explants (five donors) were infected with human seasonal influenza H3N2 virus A/Panama/2007/1999 (IAV) (orange), Middle East respiratory syndrome coronavirus (MERS-CoV) (blue), SARS-CoV (green) and SARS-CoV-2 (red) with 1×10^6 plaque-forming units (PFU) and viral replication was assessed. b) Human lung tissue explants (four donors) were infected with IAV H3N2 (orange), MERS-CoV (blue), SARS-CoV (green) with 1×10^6 PFU and SARS-CoV-2 (red) with 30×10^6 PFU and viral replication was measured showing validation of figure 3a for all viruses and loss of significance for SARS-CoV-2. External validation experiment of SARS-CoV-2 replication (three donors) is shown in supplementary figure S3a. c) Calu-3 cells were infected with IAV H3N2 (orange), MERS-CoV (blue), SARS-CoV (green) and SARS-CoV-2 (red) with multiplicity of infection (MOI) 0.1 and viral replication was assessed. d) ACE2 expression (Western blot) in wild-type human bronchial organoids (wt), organoids with lentiviral transduction and overexpression of ACE2 ($ACE2^+$) and Calu-3 cells. β-Actin served as loading control. e) ACE2 immunostaining (green) and *in situ* hybridisation (red) in human $ACE2^+$ bronchial organoids (left panel) showing abundant *ACE2* mRNA expression with a sub-fraction of cells positive for apical ACE2 protein expression. The right panel demonstrates a partly apical expression of ACE2 in $ACE2^+$ bronchial organoids as well as a congruency for SARS-CoV-2 S-protein detection in these cells (16 h post-infection, MOI 1). Cell nuclei are visualised by 4′,6-diamidino-2-phenylindole (DAPI) stain (blue). Scale bar=10 µm. f) Wild-type (wt) and ACE2 overexpressing ($ACE2^+$) bronchial organoids (four independent experiments) were infected with SARS-CoV-2 with MOI 1 and viral replication was measured after 0, 16, 24, 48 and 72 h depicting no permissiveness for SARS-CoV-2 when ACE2 is missing and increased permissiveness after ACE2 overexpression. g) Wild-type (wt) alveolar organoids (six independent experiments) were infected with SARS-CoV-2 with MOI 1 and viral replication was measured after 0, 24, 48 and 72 h. h) Uniform Manifold Approximation and Projection embedding of alveolar and bronchial organoid data shows cells positive for SARS-CoV-2 (red). i) ACE2 immunostaining (green, arrows show apical ACE2 expression in SARS-CoV-2 infected cells) and SARS-CoV-2 S-protein detection (red) in human alveolar organoids (24 h post-infection, MOI 1, three independent experiments). Cell nuclei are visualised by DAPI stain (blue). Scale bar: 10 µm. Data are presented as mean±SEM. *: p<0.05, **: p<0.01, ***: p<0.001.

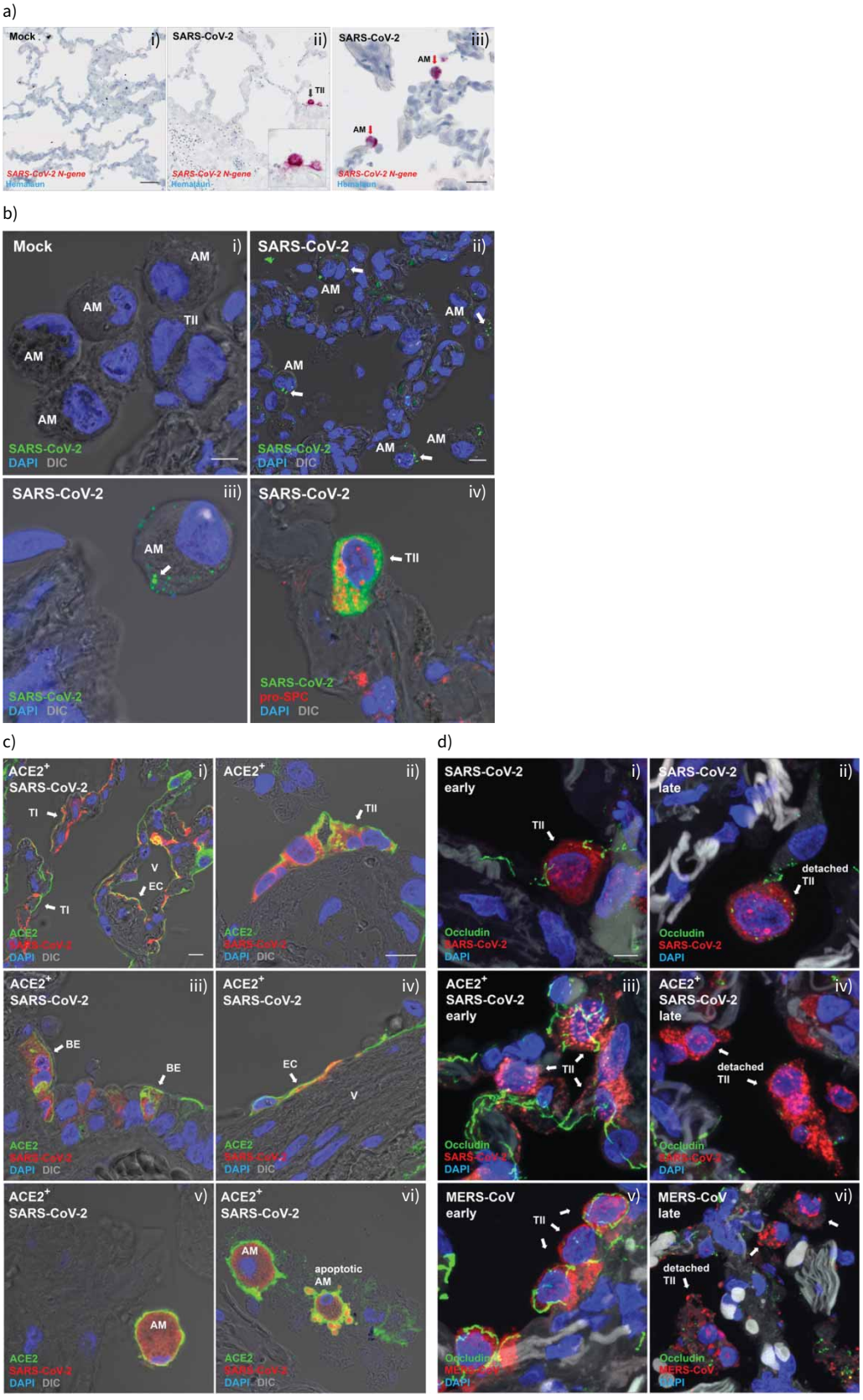

FIGURE 4 Severe acute respiratory syndrome coronavirus 2 (SARS-CoV-2) has a rare tropism to alveolar epithelial type 2 (AT2), but is frequently phagocytosed by alveolar macrophages (AM) in *ex vivo* infected human lungs. a) *In situ* hybridisation for *N-gene* of SARS-CoV-2 (red) in mock-infected (panel i) and SARS-CoV-2

infected (30×10^6 plaque-forming units (PFU); panels ii and iii) human lung tissue. Black arrows indicate AT2 cells (TII) and red arrows alveolar macrophages. Cell nuclei are visualised by Hemalaun stain (blue). Scale bars: 50 µm (panels i and ii), 20 µm (panel iii). b) Spectral imaging of immunostained SARS-CoV-2 (N-protein, green) in mock-infected (panel i) and SARS-CoV-2-infected (30×10^6 PFU; panel ii, iii and iv) human lung tissue confirms rare AT2 tropism, but punctuated viral staining pattern in AM. AT2 cells (TII) and AM are indicated in panels i, ii and iii. Pro-surfactant protein C staining (red) was used in panel iv as AT2 marker. Cell nuclei are visualised by 4′,6-diamidino-2-phenylindole (DAPI) stain (blue). Scale bars: 5 µm (panels i, iii and iv), 10 µm (panel ii). c) Overexpression of angiotensin-converting enzyme 2 (ACE2) ($ACE2^+$, green) in human lung tissue results in broadening of $ACE2^+$ cell types. ACE2-positive AT1 (TI, panel i), endothelial cells (EC, panels i and iv), AT2 (TII, panel ii), bronchial epithelium (BE, panel iii) and AM (panels v and vi) show correlation with SARS-CoV-2 infection (red). Cell nuclei are visualised by DAPI stain (blue). Scale bars: 10 µm. d) Occludin lining and loss (green) indicate virus-induced tissue damage, which is moderate at early and late stages of SARS-CoV-2 infection in human lung tissue (panels i and ii). Overexpression of ACE2 ($ACE2^+$) in human lungs leading to a broadened cellular tropism of SARS-CoV-2 (panel iii) results in an increase of cellular damage at late stages of infection (panel iv), similar to Middle East respiratory syndrome coronavirus (MERS-CoV) (panels v and vi). Cell nuclei are visualised by DAPI stain (blue). Scale bars: 5 µm. MERS-CoV immunostaining and *in situ* hybridisation in human lung tissue and SARS-CoV-2 immunostaining and *in situ* hybridisation in Calu-3 cells as well as control staining for $ACE2^+$ and occludin are presented in supplementary figure S4.

up to several weeks, one case (P1) underwent early death (6 days post-diagnosis) after compassionate best supportive care. *In situ* hybridisation on P1 lung sections revealed several SARS-CoV-2-positive cells within the alveoli, weaker signs of immune cell infiltration and alveolar epithelial damage (figure 5a and supplementary figure S5c). Most SARS-CoV-2-positive cells resembled alveolar macrophages as well as some AT2 cells. We found punctuated staining pattern of SARS-CoV-2 S-protein in alveolar macrophages, similar to *ex vivo* infected lungs as well as a strong cytosolic signal in a minor fraction of AT2 cells (figure 5b). SARS-CoV-2-positive AT2 cells were found to be endocytosed by alveolar macrophages. Similar to scarce ACE2 immunostaining of *ex vivo* lung tissue, ACE2 protein in infected areas of the autopsy lung was even undetectable, compared to highly positive autopsy kidney (same patient, supplementary figure S5d).

SARS-CoV-2 leads to immune activation by induction of inflammatory alveolar macrophages

To further elucidate the impact of SARS-CoV-2 infection in alveoli, we analysed infected explant and autopsy lungs (figure 3a, b) by bulk RNA sequencing, scSeq and snSeq (figures 6 and 7, supplementary figures S6 and S7). In line with replication data (plaque assay), we found high levels of viral reads for IAV and MERS-CoV, while SARS-CoV and SARS-CoV-2 RNA were poorly detectable by bulk RNA sequencing on lung explants (supplementary figure S6a) (16 h post-infection, equal viral input 1×10^6 plaque-forming units (PFU); figure 3a, supplementary table S1). Analysis of subgenomic viral RNA indicating active replication [49] showed appreciable levels for MERS-CoV, but only low levels for SARS-CoV or SARS-CoV-2 (supplementary figure S6a). Infection of explants by SARS-CoV or SARS-CoV-2 resulted in a weak gene expression response (supplementary figure S6b) with very few differentially expressed genes (supplementary figure S6b, supplementary table S4) in bulk transcriptomic data. Specifically, we observed a lack of characteristic antiviral gene expression signatures or specific IFN response (supplementary figure S6b and c), but weak, yet significant, induction of tumour necrosis factor (TNF)-α signalling (supplementary figure S6b, supplementary table S4). No significant change in gene expression for *ACE2*, *BSG*, *TMPRSS2* or *FURIN* was detected (supplementary figure S6c). In contrast, IAV and MERS-CoV infection induced robust and distinguishable transcriptomic responses, *e.g.* upregulation of virus response genes such as *OAS1*, *MX1/2* and IFN-related pathways (supplementary figure S6b).

To further dissect SARS-CoV-2 tropism and transcriptional response to infection, we performed scSeq of lungs infected with high virus load for SARS-CoV-2 (figures 3b, 6 and supplementary figure S6). We combined single-cell data from uninfected control tissue with another 21 samples infected with IAV, MERS-CoV, SARS-CoV (1×10^6 PFU each), or SARS-CoV-2 (30×10^6 PFU). Data were integrated with snSeq data of lung autopsy material from two acute and four prolonged COVID-19 cases (supplementary table S2). Clustering of almost 150 000 cells resulted in a consistent cell type annotation (figure 6a). In lung explants, viral RNA from IAV and MERS-CoV was found in all cell types, but SARS-CoV and SARS-CoV-2 RNA was detected mainly in alveolar macrophages and a subpopulation of monocytes in line with microscopic analysis of *ex vivo* infected lung tissue and autopsy samples (figure 6b). The rare detection of SARS-CoV-2 in AT2 cells appeared independent of *ACE2* mRNA expression (figure 6b) [50].

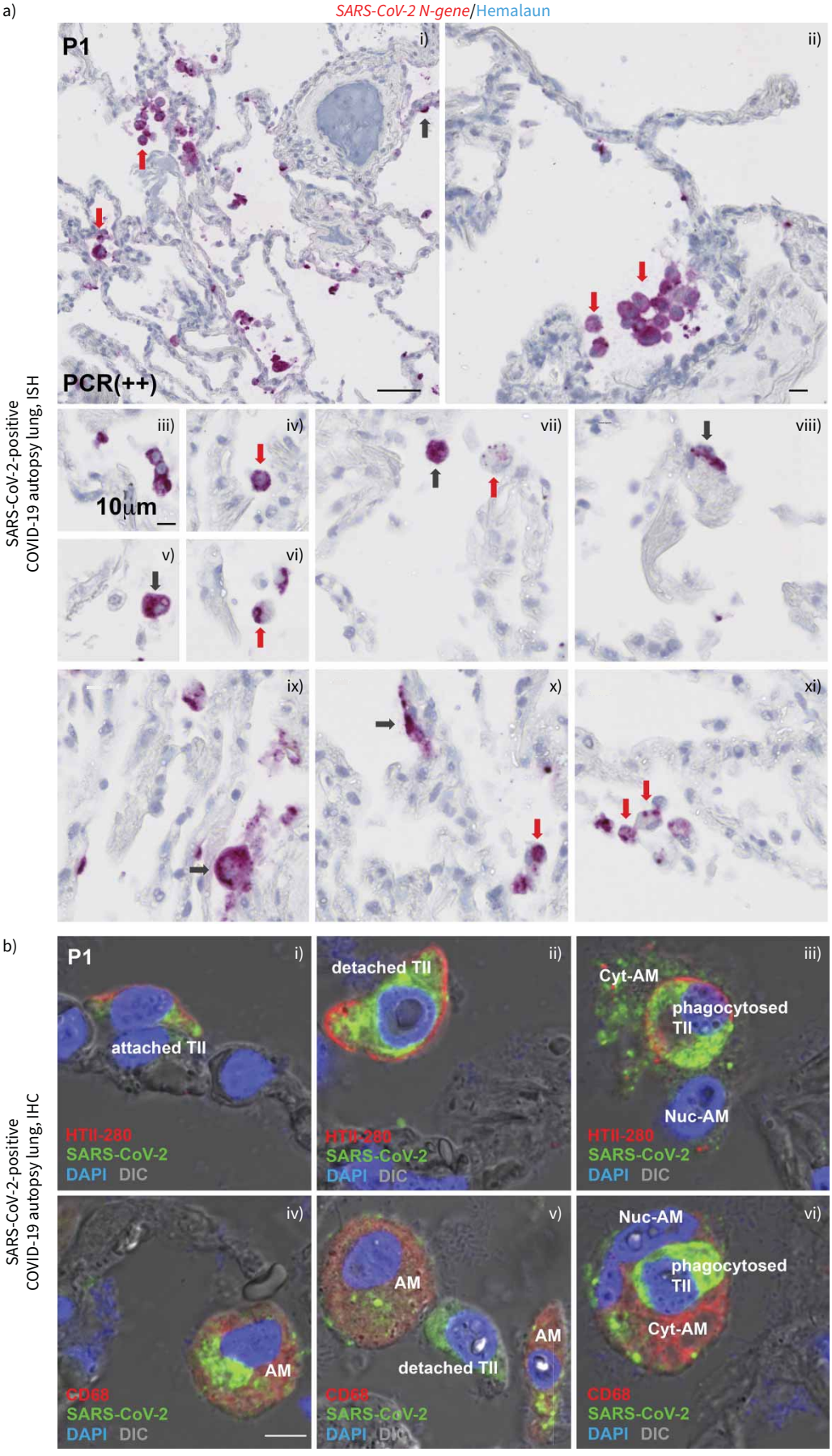
a)
SARS-CoV-2 N-gene/Hemalaun
SARS-CoV-2-positive COVID-19 autopsy lung, ISH
P1
i)
ii)
PCR(++)
iii)
iv)
10µm
vii)
viii)
v)
vi)
ix)
x)
xi)
b)
SARS-CoV-2-positive COVID-19 autopsy lung, IHC
P1
i)
attached TII
HTII-280
SARS-CoV-2
DAPI DIC
detached TII
ii)
Cyt-AM
phagocytosed TII
Nuc-AM
iii)
iv)
AM
CD68
v)
vi)

FIGURE 5 Severe acute respiratory syndrome coronavirus 2 (SARS-CoV-2) detection in alveolar macrophages and fewer alveolar epithelial type 2 (AT2) cells in lungs of an early coronavirus disease 2019 (COVID-19) death. a) *In situ* hybridisation for *N-gene* of SARS-CoV-2 (red) in an autopsy lung 5 days after COVID-19 diagnosis. Black arrows indicate AT2 cells and red arrows alveolar macrophages (AM). Cell nuclei are visualised by Hemalaun stain (blue). Scale bars: 50 µm (panel i), 10 µm (panels ii–xi). Additional donors of SARS-CoV-2-positive COVID-19 autopsy lungs and non-COVID-19 autopsy lungs are shown in supplementary figure S5. Infected areas show highly positive cells, but lack of inflammatory cell infiltration indicated by free alveoli and well-shaped alveolar septa. b) Immunolabelling of AT2 cells with HTII-280 (red, TII; panels i, ii and iii), AM with CD68 (red, AM; panels iv, v and vi) and SARS-CoV-2 (green; panels i–vi). Cytosolic staining pattern of AT2 indicate productive infection, whereas the punctuated patterns in AM indicate viral uptake. Note that infected AT2 (TII) detach from the basal membrane (panel ii) and get endocytosed by AM (panels iii and vi). Cell nuclei are visualised by 4′,6-diamidino-2-phenylindole (DAPI) stain (blue). Scale bar: 5 µm. Control staining on autopsy material as well as all other cases are shown in supplementary figure S5.

For snSeq data from autopsy samples, it is challenging to distinguish cytoplasmic viral RNA from background ambient RNA to confidently identify virus-positive cells. Therefore, we compared the fraction of virus-positive cells before and after filtering of ambient RNA (CellBender) [50, 51] and found SARS-CoV-2 viral RNA just in the acute cases and predominantly in alveolar macrophages (figure 6d). Analysis suggested that viral reads in the autopsy data in cells other than macrophages most likely originated from background RNA. Using filtered data, we consistently identified alveolar macrophages as the predominant virus-positive cell type both in lung explants and autopsy material (figure 6c) [50].

Next, we performed differential gene expression analysis between infected explants or autopsy lungs against respective controls (supplementary table S5). Expression of host factors *ACE2*, *BSG/CD147*, *TMPRSS2* and *FURIN* remained stable, with consistently low levels of *ACE2* (figure 6d). Factors such as *NRP1* [52, 53] or *DPP4* [54] showed abundant expression in several lung cell types. In contrast to the bulk RNA sequencing data, we now observed strong induction of inflammatory and antiviral genes in several cell types of the lung explants as well as the acute (virus-positive) autopsy samples (supplementary figure S6f).

Gene set enrichment analysis and summarised gene expression for antiviral and inflammatory pathways (figure 6e) revealed that *OAS* and *RIG-I* antiviral response, IFN and cytokine signalling, as well as inflammatory response was upregulated in AT2 cells, alveolar macrophages, endothelial cells and fibroblasts as a result of coronavirus infection, whereas the response to IAV for these pathways was more pronounced in monocytes and fibroblasts. Our data show that acute COVID-19 autopsy samples exhibit a related gene expression response to the SARS-CoV-2-infected lung explants (figure 6e). Finally, we analysed intercellular receptor–ligand signalling interactions and their differences between cases and controls and identified regulated signalling between T-cells and macrophages in the acute and prolonged autopsy cases (supplementary figure S6h). Next to typical co-stimulatory activation (CD28/CD86), we observed enhanced integrin/transforming growth factor (TGF) as well as downregulated CCL5/CCR1 signalling.

Macrophages showed strong viral uptake in explant and autopsy lungs and are considered to initiate the immune response in COVID-19. In particular, the prolonged autopsy samples showed alveolar macrophages expansion, possibly reflecting systemic monocyte/macrophage recruitment in late stages of disease (supplementary figure S6e). Differential gene expression analysis confirmed induction of IFN-stimulated genes both after MERS-CoV and SARS-CoV-2 infection, which, along with SARS-CoV, induced consistent responses in alveolar macrophages (Spearman correlation between the estimated $\log_2$ fold changes >0.69; supplementary figure S6g) differing from IAV-induced gene induction. We aimed to disentangle cell-intrinsic responses to infection from indirect signalling-mediated effects (cloglog regression [55]) to compare virus-positive (infected) against virus-negative (bystander) alveolar macrophages (supplementary figure S6i, supplementary table S6). We observed induction of genes such as *TNFAIP6*, *NFKB1* and *IL1A* as well as downregulation of the canonical alveolar macrophages marker *FABP4* in SARS-CoV-2-positive macrophages. Generally, gene induction in infected cells compared to bystanders was much less similar between the different viral strains than the response when comparing to uninfected control cells (supplementary figure S6j).

Subclustering of the macrophage fraction revealed four major cell populations for both explant and autopsy lungs (figure 7a). Marker expression and pathway analysis (figure 7b and c) showed an inflammatory subpopulation expressing high levels of cytokines, ISGs as well as classical alveolar marker genes such as

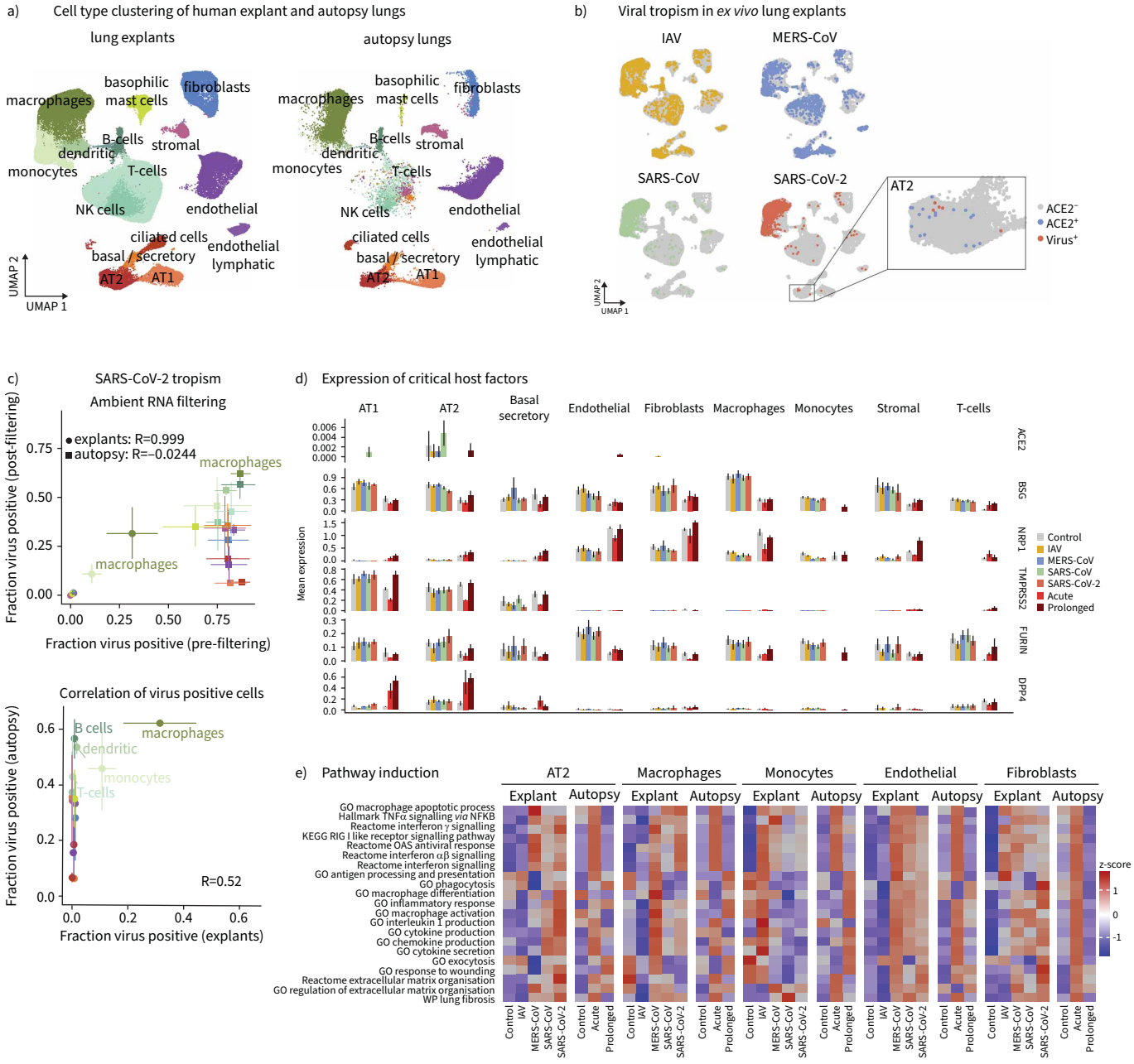

FIGURE 6 Single-cell (scSeq) and single-nucleus (snSeq) RNA sequencing reveals uptake of severe acute respiratory syndrome coronavirus 2 (SARS-CoV-2) by alveolar macrophages and inflammatory response. Human lung tissue explants infected with human seasonal influenza H3N2 virus A/Panama/2007/1999 (IAV) (orange), Middle East respiratory syndrome coronavirus (MERS-CoV) (blue), SARS-CoV (green) at 1×10^6 plaque-forming units (PFU) and SARS-CoV-2 (red) at 30×10^6 PFU as outlined in figure 3b was used for scSeq and combined with snSeq data from coronavirus disease 2019 (COVID-19) lung autopsy material. a) scSeq and snSeq of human lung tissue explants and autopsy lungs, respectively; Uniform Manifold Approximation and Projection (UMAP) embedding shows major cell types. b) UMAP embedding shows lung explant cells positive for IAV, MERS-CoV, SARS-CoV or SARS-CoV-2; inset displays SARS-CoV-2-positive alveolar epithelial type 2 (AT2) cells (red) overlaid on angiotensin-converting enzyme 2 (ACE2)-positive cells (blue). c) Quantification of virus-positive cells per cluster (colour key as in a)). Upper panel: comparing results before and after ambient RNA filtering; lower panel: comparing lung explants to lung autopsy material. Error bars represent standard deviation; Pearson correlation values are indicated. d) Quantification of the host factors *ACE2*, *CD147/BSG*, *NRP1*, *TMPRSS2*, *FURIN* and *DPP4*. Expression is averaged for all cells within one cluster of one sample, and then averaged across samples. Error bars represent standard deviation. e) Induction of antiviral and inflammatory pathways: gene expression scores for relevant pathways are averaged across all cells per cluster and condition; z-scores are computed separately for explant and autopsy data. Further analysis is presented in supplementary figure S6.

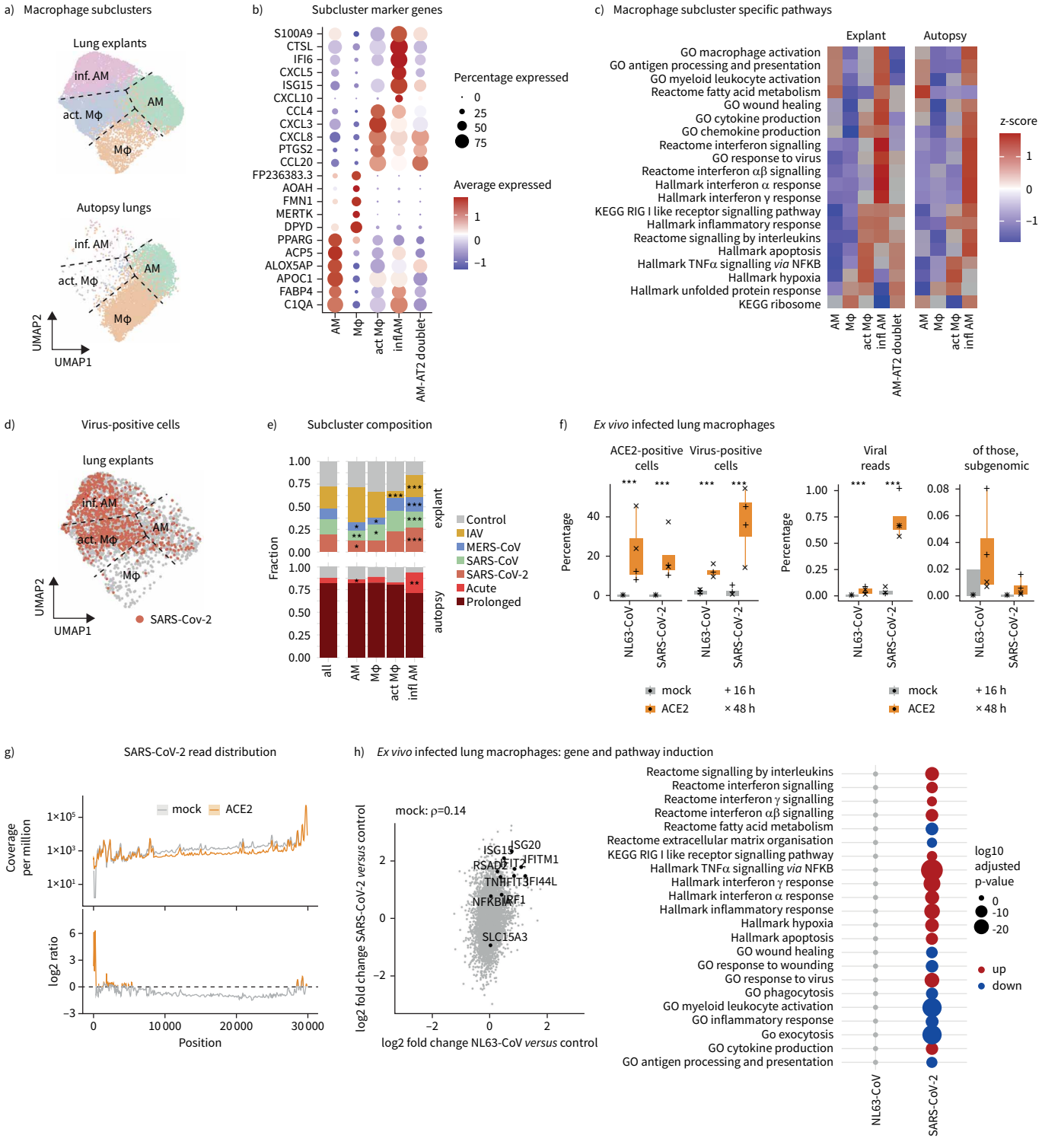

FIGURE 7 Single-cell RNA sequencing reveals inflammatory response of alveolar macrophages (AM) and nonproductive uptake in the absence of angiotensin-converting enzyme 2 (ACE2). Subclustering of macrophages from figure 6, and analysis of isolated lung macrophages infected *ex vivo* with severe acute respiratory syndrome coronavirus 2 (SARS-CoV-2) (30×10^6 plaque-forming units (PFU)) and NL63-CoV (1×10^6 PFU). a) Subclustering of macrophages reveals four subpopulations. Dashed lines serve as a guide to the eye. b) Expression of the top five marker genes for each subcluster in a). c) Gene expression scores for marker-associated pathways from b). Scores are averaged across all cells per subcluster and z-scores are computed separately for explant and autopsy data. d) SARS-CoV-2-positive cells in macrophages from lung tissue explants. e) Compositional changes of macrophage subclusters. p-values from a mixed-effects binomial model. *: p<0.05, **: p<0.01, ***: p<0.001. f) *Ex vivo* infected lung macrophages. Left panel: percentage of ACE2- or virus-positive cells infected with NL63-CoV or SARS-CoV-2 under mock treatment or ACE2

overexpression, respectively. Right panel: viral reads (as percentage of total) and subgenomic reads (as percentage of viral) for NL63-CoV and SARS-CoV-2, respectively. p-values from binomial model. ***: p<0.001. g) Distribution of reads mapping to the SARS-CoV-2 genome for *ex vivo* infected AM under mock treatment or ACE2 overexpression. Top panel: coverage per million mapped reads smoothed with 10 nt moving average. Shaded area indicates mean±SEM across replicates. Bottom panel: log2 ratio between ACE2 and mock conditions. h) Differential gene expression and pathway analysis for mock-treated *ex vivo* infected lung macrophages. Left panel: log2 fold change for NL63-CoV *versus* control plotted against log2 fold change for SARS-CoV-2 *versus* control. Interferon-stimulated genes (adjusted p<0.01) are highlighted. Right panel: pathway enrichment analysis for the log2 fold changes values with tmod [48]. Further analysis is presented in supplementary figure S7. UMAP: Uniform Manifold Approximation and Projection.

FABP4 (inflammatory alveolar macrophages). A population of activated macrophages with high levels of TNF-α signalling, but weaker induction of other pro-inflammatory genes (act. MΦ) was identified. The other two populations were assigned as classical alveolar macrophages and a more heterogeneous population of *MERTK*-positive monocyte-derived macrophages (MΦ) [56]. Interestingly, we identified rare cell doublets with mixed alveolar macrophages-AT2 phenotype in the SARS-CoV-2-infected lung explant scSeq data, more frequently than in the controls or the autopsy snSeq data, suggesting that such doublets might represent AT2 cells phagocytosed by alveolar macrophages (supplementary figure S7a; see also figure 5b). These doublets exhibited similar marker expression and pathway scores to the act. MΦ population (figure 7b and c). Furthermore, we cross-checked our results with multi-epitope ligand cartography data for the acute COVID-19 autopsy samples (11 days post-symptom onset). Indeed, macrophages identified by the typical lineage marker CD68 revealed corresponding inflammatory markers such as S100A9 and C1Q, as well as CCR2, CXCR3 and human leukocyte antigen-DR-Q (supplementary figure S7b).

Inflammatory alveolar macrophages and activated macrophage subpopulations were underrepresented in autopsy samples but contained most virus-positive cells in explant lungs (figure 7d) whereas MΦ in explant lungs were largely negative for SARS-CoV-2 (supplementary figure S7c). We found a significant depletion of the alveolar macrophages population together with an expansion of inflammatory alveolar macrophages both in lung explants and in the acute autopsy samples (figure 7e). Antiviral and inflammatory pathways as well as apoptotic genes were upregulated in inflammatory alveolar macrophages (figure 7c). Regulatory network inference (SCENIC [57]) confirmed induction of IFN-regulated factors (*IRF2*, *IRF3*, *IRF5*) in inflammatory alveolar macrophages and NF-κB/TNF signalling regulators in activated MΦ (supplementary figure S7d). Finally, we compared expression patterns of the macrophage subpopulations identified here to published scSeq and snSeq data from lung autopsies as well as bronchoalveolar lavages (BAL) [27, 50, 58, 59] (supplementary figure S7e and f). Besides the expected correspondences within more alveolar macrophage- and more monocyte-like populations, we found high similarity between the inflammatory alveolar macrophages population identified here and some inflammatory macrophage subtypes described previously (supplementary figure S7e). Within this group, dataset-specific gene expression, regarding cytokine induction, indicates differences between lung autopsy tissue, BAL samples and explant models at different stages of infection (supplementary figure S7f). In particular, we detected early induction of genes such as *CCL3*, *CCL20*, *CXCL5*, *CXCL8* or *IL1B* in the inflammatory macrophages of the explant lungs, which seem not to be upregulated in later stages of infection in this macrophage subtype.

Next, we corroborated these findings by *ex vivo* infection of isolated alveolar macrophages from human lungs ($ACE2^-$/$ACE2^+$) with SARS-CoV-2 or NL63-CoV, respectively [60], in order to separate gene expression changes due to productive infection or immune response. ScSeq data of ∼50 000 cells in 24 samples from two donors and two time points showed substantial differences between the conditions after accounting for variability between the donors (supplementary figure S7g and S7h). $ACE2^+$ macrophages showed increased viral load for both viruses (figure 7f). Although the levels were too low to reach statistical significance, we detected subgenomic viral RNA (figure 7f), suggesting active viral replication if alveolar macrophages express apical ACE2 (figure 4c) [49]. We exploited the increased coverage of the viral genome to inspect the genomic distribution of reads (figure 7g and supplementary figure S7i) and observed a 3′ bias as expected from the poly(A) selection strategy employed in our sequencing protocol. However, within $ACE2^+$ alveolar macrophages, we noted additional enrichment of reads near the 5′ and 3′ ends of the SARS-CoV-2 genome, confirming the presence of subgenomic viral RNA [49]. A comparison of MERS-CoV *versus* SARS-CoV-2 in lung explants (supplementary figure S7j), together with the pronounced differences in replication efficiency between MERS-CoV and SARS-CoV-2 (figure 3b), also suggests productive infection in ACE2-positive *ex vivo* alveolar macrophages only, which is in agreement with imaging data (figure 4).

While adenoviral $ACE2^+$ induction by itself induced inflammatory response genes (supplementary figure S7h), $ACE2^-$ alveolar macrophages depicted a transcriptional response to SARS-CoV-2 leading to IFN and TNFα signalling which was absent for NL63-CoV (figure 7h, supplementary table S7), corroborating our observations in lung explants and autopsy samples.

Discussion

The present study depicts that ACE2 is scarcely expressed in a minor AT2 cell fraction, which correlates with a limited ability of SARS-CoV-2 to propagate in the human alveolar compartment, inferior to IAV and MERS-CoV. Instead, our data from *ex vivo* infected human lung tissue as well as from autopsies suggest that SARS-CoV-2 virions reaching the alveolus are primarily endocytosed by alveolar macrophages leading to induction of different inflammatory phenotypes. In particular, expansion of activated MΦ and inflammatory alveolar macrophages is observed in lung explants and autopsy samples from acute COVID-19 cases, which may play different roles. Based on these results, we conclude that in severe COVID-19, virus-activated alveolar macrophages rather than virus-induced epithelial tissue damage is a central starting point of alveolar pathogenesis. Presumably, the patient-specific risk factors and the absolute viral load play a role in determining whether a well-regulated or dysregulated immune response develops. Moreover, our infection experiments of alveolar macrophages ($ACE2^-$/$ACE2^+$) indicate nonproductive SARS-CoV-2 uptake along with induction of antiviral and inflammatory response pathways.

Based on the study of Hamming *et al.* [12] as well as some more recent studies, a constitutively high or comorbidity-induced ACE2 expression should be expected within the alveolar compartment, leading to significant SARS-CoV-2 replication with resulting severe viral pneumonia and ARDS [12–18]. Interestingly, other recent studies revealed opposite findings and claimed a rather low alveolar ACE2 expression [11, 14, 19–21]. These contradictory findings have raised the question whether and to what extent alveolar ACE2 matters for SARS-CoV-2 pathogenesis [9–11]. Since several of these studies focused exclusively on *ACE2* mRNA, which can be a hindrance to drawing definite conclusions, we carefully used several independent methods, models and tissue on both mRNA and protein, to elucidate the alveolar role of ACE2 [11, 20, 22–24].

Our findings regarding ACE2 suggest four major conclusions: first, *ACE2* mRNA expression does not necessarily mount into detectable ACE2 protein expression in pulmonary epithelial cells, which we demonstrate in human bronchial organoids as well as lung tissue. And only ACE2 surface positive cells were susceptible to SARS-CoV-2 infection, which we further validated by forced ACE2 expression in human alveoli and ACE2-positive alveolar organoids.

Second, in line with recent studies such as by Ortiz *et al*. [21], and others, we found no evidence of *ACE2*/ACE2 expression by other cells such as AT1 cells, endothelial cells, alveolar macrophages or monocytes, but only low levels in AT2 cells [19–21, 61]. We could therefore achieve productive SARS-CoV-2 infection only in AT2 cells and not, as described by other studies, in AT1 cells or alveolar macrophages [20, 25–27].

Third, scarce and AT2 cell-restricted ACE2, despite abundantly expressed alternative receptors such as BSG/CD147, NRP1, KREMEN1 or ASGR1, limits alveolar SARS-CoV-2 infection and tissue damage as shown by "ACE2 gain of function" experiments in bronchial organoids and lung tissue [39, 42, 52, 53]. Notably, only if ACE2 expression in lung tissue is forced by overexpression to various other cell types including AT1 cells, macrophages and endothelium, a broadened SARS-CoV-2 tropism as well as an increased alveolar damage similar to the level of MERS-CoV can be observed [45]. This is of particular interest suggesting that permissiveness for the virus should be judged against direct evidence for ACE2 protein. Thus, while IAV H3N2 and MERS-CoV show substantial replication in human lung tissue, correlating with abundant corresponding receptor expressions, the low ACE2 expression limits permissiveness of the human alveolus for SARS-CoV-2 as well as SARS-CoV [44–46]. In further support of our hypothesis that it is primarily ACE2, and not alternative abundantly expressed receptors such as BSG/CD147, NRP1, KREMEN1 or ASGR1, that limit the tropism of SARS-CoV-2 in the human lung, a rapid saturation of the replication rate even for strongly increased viral load showed that the virus is not able to propagate in the human lung without sufficient ACE2 [8].

Fourth, although *ACE2* mRNA was slightly induced by IFNβ, neither direct IFN stimulation nor indirectly induced IFNs by viral infection of IAV, SARS-CoV, SARS-CoV-2 or MERS-CoV could increase ACE2 protein in human lungs, as suggested by Ziegler *et al*. [18]. Likewise, no difference of ACE2 was found in autopsy lungs, which led us conclude that IFN-driven ACE2 induction is unlikely to foster disease severity. This mismatch in slight *ACE2* induction without increase of protein expression could probably be

explained by the finding of Onabajo *et al*. [62], who demonstrated the truncated ACE2 receptor δACE2 as the actual ISG. The δACE2 lacks several hundred amino acids at the N-terminus, thereby abolishing S-protein binding and cellular–viral fusion. These data show that further in-depth studies are needed to determine isoforms, regulatory mechanisms and the definite role of ACE2 domains regarding course of COVID-19.

Regarding the cellular tropism of SARS-CoV-2, spectral microscopic analyses of *in situ* hybridisation and immunohistochemistry against *N*-/*S*-genes as well as corresponding viral proteins revealed very few virus-positive AT2 cells in lung explants and autopsy samples, which supports the findings of Hou *et al*. [20]. However, in contrast to Hui *et al*. [26], the use of highly sensitive spectral imaging revealed a distinct punctuated pattern for SARS-CoV-2 in alveolar macrophages, including autopsy samples. This punctuate staining in wild-type alveolar macrophages, in contrast to the even cytosolic distribution in AT2 and $ACE2^{+}$-alveolar macrophages, is a morphological indicator of nonproductive *versus* productive infection and raises another question [9]: if limited presence of ACE2 in human AT2 cells allows only few replicative niches for SARS-CoV-2 with only minor virus-induced tissue damage, which mechanisms trigger severe inflammation of this compartment? Several studies so far have detected SARS-CoV-2 in lung monocytes and macrophages, arriving at different conclusions regarding immune activation and productive infection of these cells [27, 50, 58, 59, 63–66]. Therefore, we tested the hypothesis that these cells adopt a very early pro-inflammatory phenotype as result of viral uptake rather than productive infection. Results from lung explants and autopsy indicate that SARS-CoV-2 RNA is predominantly found in macrophages, but rarely in other cell types, while IAV or MERS-CoV RNA is present in almost all cell types. Comparison of macrophages from acute COVID-19 individuals and the explant model showed consistent activation of several pathways including chemo-/cytokine production, IFN signalling and response, TNF/NF-κB signalling and apoptosis. An in-depth characterisation of macrophage subclusters in autopsy samples and explants further revealed a strong activated as well as inflammatory phenotype, which increase in abundance in the SARS-CoV-2 infected explants as well as in acute autopsy cases.

Whereas activated MΦ seem to obtain their phenotype mainly by phagocytosis of infected and apoptotic AT2 cells, endocytosis of SARS-CoV-2 virions predominantly induces the inflammatory alveolar macrophage phenotype, which is not present after uptake of NL63-CoV. Interestingly, this inflammatory activation seems independent of productive SARS-CoV-2 infection since SARS-CoV-2 subgenomic RNA was only noticed by ACE2 overexpression ($ACE2^{+}$-alveolar macrophages) and not in the wild-type alveolar macrophage population [64, 65]. In this regard, our conclusions differ from Grant *et al*. [27] who used negative strand (antisense) viral RNA as indicator for productive infection. In our data, we found antisense RNA at similar levels in well-expressed housekeeping genes, probably due to limited strand specificity in library preparation. Likewise, infection neither with SARS-CoV-2 or the well-replicating MERS-CoV resulted in an increase of viral antisense RNA above this technical background level. Additionally, our conclusion is supported by a Syrian hamster model, in which SARS-CoV-2 uptake without productive infection is frequently observed, leading to strong activation of macrophages [67]. Experiments in mice indicate that the detection of SARS-CoV-2 spike protein may be important for alveolar macrophage activation [68], and co-stimulation of alveolar macrophages with low fucosylated anti-spike IgG in early COVID-19 may further fuel subsequent development of lung damage [69]. Together, these data indicate that uptake of SARS-CoV-2 induces (next to activated MΦ) an inflammatory alveolar macrophages phenotype characterised by a subsequent pro-inflammatory response, although not driven by productive infection, probably contributing to severe lung and systemic inflammation dependent on underlying individual risk factors such as gender, age and comorbidities.

Indeed, a drawback of the explant model is that infection and pro-inflammatory activation of alveolar macrophages does not allow for recruitment of further immune cells such as neutrophils or T-cells. However, by analyses of intercellular receptor–ligand interactions in the acute and prolonged autopsy cases we identified several up- and downregulated signalling pathways, which are probably the outcome of the pro-inflammatory activation [70]. The identified integrin/TGF axis in COVID-19 has been associated with triggering vascular leakage and its blockage could attenuate viral replication in the airway epithelium [71, 72]. In addition, the identified low *CCL5* together with high viral load may direct to severe outcome in COVID-19 [73]. And although a benefit for the *CCL5*/*CCR1* axis disruption for COVID-19 outcome has been described, its functional role is so far not elucidated [74]. These and other signalling pathways need to be considered and analysed in detail in subsequent studies.

Further factor specific analysis of SARS-CoV-2-positive alveolar macrophages revealed, compared to bystander cells, induction of endosomal TLR8 or the NLRP3 inflammasome activator P2X7 receptor (*P2RX7*), which may support subsequent cytokine and chemokine release [75, 76]. Notably, a recent study

indicated NLRP3 inflammasome activation in human primary monocytes exposed to SARS-CoV-2 and CD14-positive cells in lung autopsy samples [76, 77]. In (virus-positive) macrophages, P2X7R is part of the STING signalling cascade [78], and SARS-CoV-2 seems to initiate cGAS-STING-related macrophage activation [79], which may contribute to COVID-19 immunopathology [80]. Along those lines, detection of SARS-CoV-2 N-protein may further aggravate inflammation by inflammasome activation [81].

The observed upregulation of NFKB1 could further detrimentally enhance inflammation, since inhibition of this pathway reduced lung inflammation and increased survival in SARS-CoV infected mice [82]. Severe inflammation caused by macrophage expression of cyclooxygenase-2 (*PTGS2*) contributed to avian H5N1 infection [83] and we noted pronounced *PTGS2* upregulation in SARS-CoV-2-positive alveolar macrophages. In line, upregulation of myristoylated alanine-rich C kinase substrate (*MARCKS*) may contribute to increased macrophage pro-inflammatory cytokine expression [84], and we indeed noted increased expression of interleukin-1α (*IL1A*) [85]. Upregulated molecules such as *MARCKS* and proline-serine-threonine phosphatase-interacting protein 2 (*PSTPIP2*) may increase the directed migration of those cells [86]. In H1N1 IAV-infected mice fatty acid binding protein 5 (*FABP5*)-deficiency caused excessive inflammation and we noted reduced *FABP5* presence in SARS-CoV-2-positive macrophages [87] indicating that downregulation of genes in macrophages may also contribute to enhanced inflammation. Conversely, augmented expression of TNF-α-induced protein 6 (*TNFAIP6*) in SARS-CoV-2-positive alveolar macrophages may counter-regulate excessive inflammation, since deletion of this molecule in mice augmented inflammatory lung injury and mortality in an acute lung injury model [88].

Since several studies already reported monocyte/macrophage activation in COVID-19, we compared our annotated monocyte/macrophage datasets with that of the studies by Grant *et al*. [27], Liao *et al*. [58], Delorey *et al*. [50] and Wendisch *et al*. [59]. As expected, tissue-resident macrophages, monocytes and inflammatory macrophages are found with similar signatures in all datasets. However, relative comparison of inflammatory chemo- and cytokine induction in the inflammatory alveolar macrophages phenotype shows a different focus among the datasets. In particular, in the inflammatory alveolar macrophages of the explant lungs early induction of, *e.g.* CCL3, CCL20, CXCL5, CXCL8 or interleukin-1β was detected, which seem less upregulated in later stages of infection, thereby reflecting the very early (immediately after virus ingestion) response in alveolar macrophages probably responsible for recruitment of systemic immune cells and further activation [89–92].

Thus, the observed pro-inflammatory phenotype of macrophages observed in our study (and other reports) may contribute to severe COVID-19 by creating a strong local pro-inflammatory environment contributing to alveolar malfunction, including impaired barrier function and endothelial activation [77, 93, 94]. Subsequent endothelial activation fuelled by the pro-inflammatory macrophages may result in the reduction of thromboprotective mechanisms, thereby promoting local coagulation [95, 96]. Indeed, increased expression of pro-coagulant markers, and chemokines in endothelial cells was noted in endothelium exposed to the culture medium of monocytes pre-incubated with SARS-CoV-2 spike S1 protein [97].

Studies of autopsy specimens from deceased COVID-19 patients suggest complex activation of various pro-inflammatory phenomena, some of which are based on direct local tissue responses, which in turn are highly dependent on recruited cells or systemic factors (*e.g.* complement) [97]. Of note, even within severe COVID-19 courses, there can be considerable variation in the manifestation of the disease [7] and it is still unclear why severe COVID-19 results in some specific disease features, such as the massive occurrence of microthrombi in small vessels, that do not occur in classical ARDS. Similarly, it is important to clarify why other diseases with comparable activation of alveolar macrophages have a different phenotype and which factors ultimately determine the specific susceptibility of patient subgroups to severe COVID-19.

Collectively, our data strongly support our conclusion that, due to scarce alveolar ACE2 expression, direct SARS-CoV-2 infection of AT2 cells and related tissue damage is probably not the driving force for an overwhelming cytokine release and macrophage inflammation leading to severe courses of COVID-19. When significant amounts of SARS-CoV-2 viruses may reach the alveoli from the upper respiratory tract, their uptake by alveolar macrophages induces specific pro-inflammatory phenotypes that appear to trigger the subsequent systemic responses. This presumably occurs without relevant viral replication, initial tissue damage and release of epithelial-derived danger-associated molecular patterns. However, the specific and strong induction of inflammatory macrophage phenotypes cannot alone explain which patients progress to severe disease. Therefore, individual risk factors in large cohorts need to be correlated with the specific activated pathways of macrophage subtypes.

Acknowledgements: The authors thank Doris Frey, Lisa Skrip and Gudrun Heinz for excellent technical assistance as well as Jeannine Wilde, Tatiana Borodina, Daniele Sunaga-Franze and Madlen Sohn from the MDC/BIH sequencing facility.

Raw data are available from the corresponding author upon reasonable request. Processed sequencing data have been deposited in GEO under accession number GSE198864. Analysis code and scripts to generate associated figures are accessible at https://github.com/bihealth/hoenzke_et_al_human_lungs_covid_ace2.

Author contributions: K. Hoenzke, C. Mache, D. Fathykova, M. Kessler, S. Dökel, K. Hoffmann, M. Baumgardt, J. Schulze, B. Biere, M. Mieth, K. Hellwig, A. Mecate-Zambrano, A. Löwa, P. Graff, Z. Demir and L. Brunotte performed and analysed experiments. E. Wyler performed sequencing and contributed to data analysis supervised by M. Landthaler. B. Obermayer performed analysis of sequencing data, supervised by D. Beule. J. Bushe and A.D. Gruber performed the processing for histology and immunofluorescence and supported with probe design. M. Dohmen carried out the computational analysis of the pathology samples. S. Elezkurtaj, F. Klauschen, D. Horst, H. Radbruch, J. Radke and F. Heppner provided the pathological patient samples. M. Tönnies, T.T. Bauer, S. Eggeling, H-L. Tran, P. Schneider, J. Neudecker and J.C. Rückert provided the lung tissue explants and related meta-data. C. Hinze, J. Busch and K.M. Schmidt-Ott provided kidney tissue and protein. D. Niemeyer, C. Drosten, M.A. Müller, V.M. Corman and C. Goffinet were responsible for virus sequencing, qPCR and virus stock preparation. A.E. Hauser, R. Mothes and A. Pascual-Reguant performed the MELC studies. T. Wolff, S. Hippenstiel, N. Suttorp, S. Ludwig, M. Witzenrath and L-E. Sander provided conceptual advice. A.C. Hocke, K. Hoenzke and B. Obermayer wrote the manuscript. A.C. Hocke conceived and supervised the study. All authors revised and approved the final version of the manuscript.

Conflict of interest: J-C. Rückert and H. Radbruch report support from DFG RA 2491/1-1, BMBF (Defeat Pandemics). A.E. Hauser reports support from Charité – Universitätsmedizin Berlin and Deutsches Rheuma-Forschungszentrum Berlin, and grants from Deutsche Forschungsgemeinschaft (HA5354/10-1, TRR130,P17 and C01, HA5354/8-1). T. Wolff reports support from Federal Ministry of Education and Research (BMBF) grant 01K12006F. M. Kessler reports grants from BMBF Organo-Strat, Einstein 3R. M. Dohmen reports contracts with Max-Delbrück Center, Berlin; grants from Gender Equality Fund, Berlin Institute of Health. F. Klauschen reports consulting fees, lecture honoraria, travel support and participation on advisory boards with BMS, Novartis, Roche and Lilly, and is a co-founder of AI-BIH/Charité-Spinoff Aignostics GmbH. F. Heppner reports consulting fees, lecture honoraria, payment for expert testimony and leadership roles at Novartis, AstraZeneca and ThinkHealth Hygiene Solutions. V.M. Corman reports the following patents: 20210190797 (Methods and reagents for diagnosis of SARS-CoV-2 infection); 9841834 (Human recombinant monoclonal antibody against SARS-CoV-2 spike glycoprotein); 9909654 (A pharmaceutical combination comprising an anti-viral protonophore and a serine protease inhibitor). D. Niemeyer reports that Technische Universität Berlin, Freie Universität Berlin and Charité – Universitätsmedizin have filed a patent application for siRNAs inhibiting SARS-CoV-2 replication with D. Niemeyer as coauthor. M.A. Müller reports the following patents: 20210190797 (Methods and reagents for diagnosis of SARS-CoV-2 infection); 9841834 (Human recombinant monoclonal antibody against SARS-CoV-2 spike glycoprotein); 9909654 (A pharmaceutical combination comprising an anti-viral protonophore and a serine protease inhibitor); and has participated on an advisory board for ECDC/WHO. S. Ludwig reports consulting fees from Atriva Therapeutics GmbH, Biontec SE; and has patent PCT/EP2021/063485 pending. M. Witzenrath reports grants from Deutsche Forschungsgemeinschaft, Bundesministerium für Bildung und Forschung, Deutsche Gesellschaft für Pneumologie, European Respiratory Society, Marie Curie Foundation, Else Kröner Fresenius Stiftung, Capnetz Stiftung, International Max Planck Research School, Quark Pharma, Takeda Pharma, Noxxon, Pantherna, Silence Therapeutics, Vaxxilon, Actelion, Bayer Health Care, Biotest and Boehringer Ingelheim; consulting fees from Noxxon, Pantherna, Silence Therapeutics, Vaxxilon, Aptarion, GlaxoSmithKline, Sinoxa and Biotest; lecture honoraria from AstraZeneca, Berlin Chemie, Chiesi, Novartis, Teva, Actelion, Boehringer Ingelheim, GlaxoSmithKline, Biotest, Bayer Health Care; and has the following patents issued: EPO 12181535.1 (IL-27 for modulation of immune response in acute lung injury), WO/2010/094491 (Means for inhibiting the expression of Ang-2), DE 102020116249.9 (Camostat/Niclosamide cotreatment in SARS-CoV-2 infected human lung cells). All other authors have nothing to disclose.

Support statement: A.C. Hocke, L-E. Sander and S. Hippenstiel were supported by Berlin University Alliance GC2 Global Health (Corona Virus Pre-Exploration Project). A.C. Hocke, S. Hippenstiel, T. Wolff and C. Drosten were supported by BMBF (RAPID), and A.C. Hocke and S. Hippenstiel by BMBF (alvBarriere-COVID-19). K. Hoenzke, L. Brunotte, S. Ludwig, S. Hippenstiel, C. Drosten, C. Goffinet, T. Wolff and A.C. Hocke were funded by BMBF (NUM-COVID 19, Organo-Strat 01KX2021). K. Hoenzke, N. Suttorp, L-E. Sander, M. Witzenrath, S. Hippenstiel, A.D. Gruber, C. Drosten, T. Wolff and A.C. Hocke were supported by DFG (SFB-TR 84). A.C. Hocke was supported by BIH and Charité-Zeiss MultiDim. A.C. Hocke and S. Hippenstiel were supported by Charite 3R. K. Hoenzke, A.C. Hocke, M. Kessler, A.D. Gruber and S. Hippenstiel were supported by Einstein Foundation EC3R. K. Hoenzke and C. Drosten were supported by BMBF (Camo-COVID-19). M. Witzenrath, N. Suttorp and S. Hippenstiel were

supported by BMBF (PROVID). C. Goffinet and A.C. Hocke were funded by BIH. M. Witzenrath and N. Suttorp were supported by BIH and BMBF (SYMPATH, CAPSyS, NAPKON). B. Obermayer and D. Beule were funded through the BIH Clinical Single Cell Bioinformatics Pipeline. Computation was performed on the HPC for Research cluster of the Berlin Institute of Health. L. Brunotte was supported by the BMBF (CoIMMUNE), the DFG (KFO 342) and the IZKF of the Medical Faculty of the WWU. A.E. Hauser, R. Mothes and A. Pascual-Reguant were supported by funding from the DFG, HA5354/10-1, SPP1937 (HA5354/8-2) and TRR130 P17. H. Radbruch was supported by DFG (RA 2491/1-1). Funding information for this article has been deposited with the Crossref Funder Registry.

References

1 Bellani G, Laffey JG, Pham T, *et al.* Epidemiology, patterns of care, and mortality for patients with acute respiratory distress syndrome in intensive care units in 50 countries. *JAMA* 2016; 315: 788–800.
2 Cummings MJ, Baldwin MR, Abrams D, *et al.* Epidemiology, clinical course, and outcomes of critically ill adults with COVID-19 in New York City: a prospective cohort study. *Lancet* 2020; 395: 1763–1770.
3 Wu C, Chen X, Cai Y, *et al.* Risk factors associated with acute respiratory distress syndrome and death in patients with coronavirus disease 2019 pneumonia in Wuhan, China. *JAMA Intern Med* 2020; 180: 934–943.
4 Ulloa AC, Buchan SA, Daneman N, *et al.* Estimates of SARS-CoV-2 omicron variant severity in Ontario, Canada. *JAMA* 2022; 327: 1286–1288.
5 Wolter N, Jassat W, Walaza S, *et al.* Early assessment of the clinical severity of the SARS-CoV-2 omicron variant in South Africa: a data linkage study. *Lancet* 2022; 399: 437–446.
6 Milross L, Majo J, Cooper N, *et al.* Post-mortem lung tissue: the fossil record of the pathophysiology and immunopathology of severe COVID-19. *Lancet Respir Med* 2022; 10: 95–106.
7 Hoffmann M, Kleine-Weber H, Schroeder S, *et al.* SARS-CoV-2 cell entry depends on ACE2 and TMPRSS2 and is blocked by a clinically proven protease inhibitor. *Cell* 2020; 181: 271–280.
8 Hofmann H, Pöhlmann S. Cellular entry of the SARS coronavirus. *Trends Microbiol* 2004; 12: 466–472.
9 Nawijn MC, Timens W. Can ACE2 expression explain SARS-CoV-2 infection of the respiratory epithelia in COVID-19? *Mol Syst Biol* 2020; 16: e9841.
10 Perrotta F, Matera MG, Cazzola M, *et al.* Severe respiratory SARS-CoV2 infection: does ACE2 receptor matter? *Respir Med* 2020; 168: 105996.
11 Zhao Y, Zhao Z, Wang Y, *et al.* Single-cell RNA expression profiling of ACE2, the receptor of SARS-CoV-2. *Am J Respir Crit Care Med* 2020; 202: 756–759.
12 Hamming I, Timens W, Bulthuis ML, *et al.* Tissue distribution of ACE2 protein, the functional receptor for SARS coronavirus. A first step in understanding SARS pathogenesis. *J Pathol* 2004; 203: 631–637.
13 Jacobs M, Van Eeckhoutte HP, Wijnant SRA, *et al.* Increased expression of ACE2, the SARS-CoV-2 entry receptor, in alveolar and bronchial epithelium of smokers and COPD subjects. *Eur Respir J* 2020; 56: 2002378.
14 Lee IT, Nakayama T, Wu CT, *et al.* ACE2 localizes to the respiratory cilia and is not increased by ACE inhibitors or ARBs. *Nat Commun* 2020; 11: 5453.
15 Li G, He X, Zhang L, *et al.* Assessing ACE2 expression patterns in lung tissues in the pathogenesis of COVID-19. *J Autoimmun* 2020; 112: 102463.
16 Pinto BGG, Oliveira AER, Singh Y, *et al.* ACE2 expression is increased in the lungs of patients with comorbidities associated with severe COVID-19. *J Infect Dis* 2020; 222: 556–563.
17 Smith JC, Sausville EL, Girish V, *et al.* Cigarette smoke exposure and inflammatory signaling increase the expression of the SARS-CoV-2 receptor ACE2 in the respiratory tract. *Dev Cell* 2020; 53: 514–529.
18 Ziegler CGK, Allon SJ, Nyquist SK, *et al.* SARS-CoV-2 receptor ACE2 is an interferon-stimulated gene in human airway epithelial cells and is detected in specific cell subsets across tissues. *Cell* 2020; 181: 1016–1035.
19 Hikmet F, Méar L, Edvinsson A, *et al.* The protein expression profile of ACE2 in human tissues. *Mol Syst Biol* 2020; 16: e9610.
20 Hou YJ, Okuda K, Edwards CE, *et al.* SARS-CoV-2 reverse genetics reveals a variable infection gradient in the respiratory tract. *Cell* 2020; 182: 429–446.
21 Ortiz ME, Thurman A, Pezzulo AA, *et al.* Heterogeneous expression of the SARS-coronavirus-2 receptor ACE2 in the human respiratory tract. *EBioMedicine* 2020; 60: 102976.
22 Lukassen S, Chua RL, Trefzer T, *et al.* SARS-CoV-2 receptor ACE2 and TMPRSS2 are primarily expressed in bronchial transient secretory cells. *EMBO J* 2020; 39: e105114.
23 Muus C, Luecken MD, Eraslan G, *et al.* Single-cell meta-analysis of SARS-CoV-2 entry genes across tissues and demographics. *Nat Med* 2021; 27: 546–559.
24 Zou X, Chen K, Zou J, *et al.* Single-cell RNA-seq data analysis on the receptor ACE2 expression reveals the potential risk of different human organs vulnerable to 2019-nCoV infection. *Front Med* 2020; 14: 185–192.
25 Chu H, Chan JF, Wang Y, *et al.* Comparative replication and immune activation profiles of SARS-CoV-2 and SARS-CoV in human lungs: an *ex vivo* study with implications for the pathogenesis of COVID-19. *Clin Infect Dis* 2020; 71: 1400–1409.

26 Hui KPY, Cheung MC, Perera R, *et al.* Tropism, replication competence, and innate immune responses of the coronavirus SARS-CoV-2 in human respiratory tract and conjunctiva: an analysis in *ex-vivo* and *in-vitro* cultures. *Lancet Respir Med* 2020; 8: 687–695.
27 Grant RA, Morales-Nebreda L, Markov NS, *et al.* Circuits between infected macrophages and T cells in SARS-CoV-2 pneumonia. *Nature* 2021; 590: 635–641.
28 Recovery Collaborative Group, Horby P, Lim WS, *et al.* Dexamethasone in hospitalized patients with Covid-19. *N Engl J Med* 2021; 384: 693–704.
29 Tomazini BM, Maia IS, Cavalcanti AB, *et al.* Effect of dexamethasone on days alive and ventilator-free in patients with moderate or severe acute respiratory distress syndrome and COVID-19: the CoDEX randomized clinical trial. *JAMA* 2020; 324: 1307–1316.
30 COVID STEROID 2 Trial Group, Munch MW, Myatra SN, *et al.* Effect of 12 mg *vs* 6 mg of dexamethasone on the number of days alive without life support in adults with COVID-19 and severe hypoxemia: the COVID STEROID 2 randomized trial. *JAMA* 2021; 326: 1807–1817.
31 Pfefferle S, Krähling V, Ditt V, *et al.* Reverse genetic characterization of the natural genomic deletion in SARS-Coronavirus strain Frankfurt-1 open reading frame 7b reveals an attenuating function of the 7b protein *in-vitro* and *in-vivo*. *Virol J* 2009; 6: 131.
32 Muth D, Meyer B, Niemeyer D, *et al.* Transgene expression in the genome of Middle East respiratory syndrome coronavirus based on a novel reverse genetics system utilizing Red-mediated recombination cloning. *J Gen Virol* 2017; 98: 2461–2469.
33 Tosti L, Hang Y, Debnath O, *et al.* Single nucleus and *in situ* RNA sequencing reveals cell topographies in the human pancreas. *Gastroenterology* 2021; 160: 1330–1344.
34 Osterrieder N, Bertzbach LD, Dietert K, *et al.* Age-dependent progression of SARS-CoV-2 infection in Syrian hamsters. *Viruses* 2020; 12: 779.
35 Legland D, Arganda-Carreras I, Andrey P. MorphoLibJ: integrated library and plugins for mathematical morphology with ImageJ. *Bioinformatics* 2016; 32: 3532–3534.
36 Contesso G, Mouriesse H. Le consensus anatomo-pathologique pour les facteurs de pronostic des cancers du sein [Anatomopathologic consensus for defining the prognostic factors of breast cancers]. *Pathol Biol* 1990; 38: 834–835.
37 Jackson CB, Farzan M, Chen B, *et al.* Mechanisms of SARS-CoV-2 entry into cells. *Nat Rev Mol Cell Biol* 2022; 23: 3–20.
38 Travaglini KJ, Nabhan AN, Penland L, *et al.* A molecular cell atlas of the human lung from single-cell RNA sequencing. *Nature* 2020; 587: 619–625.
39 Gu Y, Cao J, Zhang X, *et al.* Receptome profiling identifies KREMEN1 and ASGR1 as alternative functional receptors of SARS-CoV-2. *Cell Res* 2022; 32: 24–37.
40 Nienhold R, Ciani Y, Koelzer VH, *et al.* Two distinct immunopathological profiles in autopsy lungs of COVID-19. *Nat Commun* 2020; 11: 5086.
41 Singh M, Bansal V, Feschotte C. A single-cell RNA expression map of human coronavirus entry factors. *Cell Rep* 2020; 32: 108175.
42 Ulrich H, Pillat MM. CD147 as a target for COVID-19 treatment: suggested effects of azithromycin and stem cell engagement. *Stem Cell Rev Rep* 2020; 16: 434–440.
43 Mizuiri S, Ohashi Y. ACE and ACE2 in kidney disease. *World J Nephrol* 2015; 4: 74–82.
44 Berg J, Zscheppang K, Fatykhova D, *et al.* Tyk2 as a target for immune regulation in human viral/bacterial pneumonia. *Eur Respir J* 2017; 50: 1601953.
45 Hocke AC, Becher A, Knepper J, *et al.* Emerging human Middle East respiratory syndrome coronavirus causes widespread infection and alveolar damage in human lungs. *Am J Respir Crit Care Med* 2013; 188: 882–886.
46 Weinheimer VK, Becher A, Tönnies M, *et al.* Influenza A viruses target type II pneumocytes in the human lung. *J Infect Dis* 2012; 206: 1685–1694.
47 Elezkurtaj S, Greuel S, Ihlow J, *et al.* Causes of death and comorbidities in patients with COVID-19. *Sci Rep* 2021; 11: 4263.
48 Zyla J, Marczyk M, Domaszewska T, *et al*. Gene set enrichment for reproducible science: comparison of CERNO and eight other algorithms. *Bioinformatics* 2019; 35: 5146–5154.
49 Alexandersen S, Chamings A, Bhatta TR. SARS-CoV-2 genomic and subgenomic RNAs in diagnostic samples are not an indicator of active replication. *Nat Commun* 2020; 11: 6059.
50 Delorey TM, Ziegler CGK, Heimberg G, *et al.* COVID-19 tissue atlases reveal SARS-CoV-2 pathology and cellular targets. *Nature* 2021; 595: 107–113.
51 Fleming SJ, Marioni JC, Babadi M. CellBender remove-background: a deep generative model for unsupervised removal of background noise from scRNA-seq datasets. *bioRxiv* 2019; preprint [https://doi.org/10.1101/791699].
52 Cantuti-Castelvetri L, Ojha R, Pedro LD, *et al.* Neuropilin-1 facilitates SARS-CoV-2 cell entry and infectivity. *Science* 2020; 370: 856–860.

53 Daly JL, Simonetti B, Klein K, *et al.* Neuropilin-1 is a host factor for SARS-CoV-2 infection. *Science* 2020; 370: 861–865.
54 Raj VS, Mou H, Smits SL, *et al.* Dipeptidyl peptidase 4 is a functional receptor for the emerging human coronavirus-EMC. *Nature* 2013; 495: 251–254.
55 Bost P, Giladi A, Liu Y, *et al.* Host-viral infection maps reveal signatures of severe COVID-19 patients. *Cell* 2020; 181: 1475–1488.
56 Morse C, Tabib T, Sembrat J, *et al.* Proliferating SPP1/MERTK-expressing macrophages in idiopathic pulmonary fibrosis. *Eur Respir J* 2019; 54: 1802441.
57 Aibar S, González-Blas CB, Moerman T, *et al.* SCENIC: single-cell regulatory network inference and clustering. *Nat Methods* 2017; 14: 1083–1086.
58 Liao M, Liu Y, Yuan J, *et al.* Single-cell landscape of bronchoalveolar immune cells in patients with COVID-19. *Nat Med* 2020; 26: 842–844.
59 Wendisch D, Dietrich O, Mari T, *et al.* SARS-CoV-2 infection triggers profibrotic macrophage responses and lung fibrosis. *Cell* 2021; 184: 6243–6261.
60 Hofmann H, Pyrc K, van der Hoek L, *et al.* Human coronavirus NL63 employs the severe acute respiratory syndrome coronavirus receptor for cellular entry. *Proc Natl Acad Sci USA* 2005; 102: 7988–7993.
61 Aguiar JA, Tremblay BJ, Mansfield MJ, *et al.* Gene expression and *in situ* protein profiling of candidate SARS-CoV-2 receptors in human airway epithelial cells and lung tissue. *Eur Respir J* 2020; 56: 2001123.
62 Onabajo OO, Banday AR, Yan W, *et al.* Interferons and viruses induce a novel primate-specific isoform dACE2 and not the SARS-CoV-2 receptor ACE2. *Nat Genet* 2020; 52: 1283–1293.
63 García-Nicolás O, V'Kovski P, Zettl F, *et al.* No evidence for human monocyte-derived macrophage infection and antibody-mediated enhancement of SARS-CoV-2 infection. *Front Cell Infect Microbiol* 2021; 11: 644574.
64 Jiang M, Kolehmainen P, Kakkola L, *et al.* SARS-CoV-2 isolates show impaired replication in human immune cells but differential ability to replicate and induce innate immunity in lung epithelial cells. *Microbiol Spectr* 2021; 9: e0077421.
65 Zheng J, Wang Y, Li K, *et al.* Severe acute respiratory syndrome coronavirus 2-induced immune activation and death of monocyte-derived human macrophages and dendritic cells. *J Infect Dis* 2021; 223: 785–795.
66 Wang S, Yao X, Ma S, *et al.* A single-cell transcriptomic landscape of the lungs of patients with COVID-19. *Nat Cell Biol* 2021; 23: 1314–1328.
67 Nouailles G, Wyler E, Pennitz P, *et al.* Temporal omics analysis in Syrian hamsters unravel cellular effector responses to moderate COVID-19. *Nat Commun* 2021; 12: 4869.
68 Cao X, Tian Y, Nguyen V, *et al.* Spike protein of SARS-CoV-2 activates macrophages and contributes to induction of acute lung inflammation in male mice. *FASEB J* 2021; 35: e21801.
69 Hoepel W, Chen HJ, Geyer CE, *et al.* High titers and low fucosylation of early human anti-SARS-CoV-2 IgG promote inflammation by alveolar macrophages. *Sci Transl Med* 2021; 13: eabf8654.
70 Lagger C, Ursu E, Equey A, *et al.* scAgeCom: a murine atlas of age-related changes in intercellular communication inferred with the package scDiffCom. *bioRxiv* 2021; preprint [https://doi.org/10.1101/2021.08.13.456238].
71 Biering SB, de Sousa FTG, Tjang LV, *et al.* SARS-CoV-2 Spike triggers barrier dysfunction and vascular leak *via* integrins and TGF-β signaling. *bioRxiv* 2021; preprint [https://doi.org/10.1101/2021.12.10.472112].
72 Huntington KE, Carlsen L, So EY, *et al.* Integrin/TGF-β1 inhibitor GLPG-0187 blocks SARS-CoV-2 Delta and Omicron pseudovirus infection of airway epithelial cells which could attenuate disease severity. *Pharmaceuticals* 2022; 15: 618.
73 Pérez-García F, Martin-Vicente M, Rojas-García RL, *et al.* High SARS-CoV-2 viral load and low CCL5 expression levels in the upper respiratory tract are associated with COVID-19 severity. *J Infect Dis* 2022; 225: 977–982.
74 Patterson BK, Seethamraju H, Dhody K, *et al.* Disruption of the CCL5/RANTES-CCR5 pathway restores immune homeostasis and reduces plasma viral load in critical COVID-19. *medRxiv* 2020; preprint [https://doi.org/10.1101/2020.05.02.20084673].
75 Campbell GR, To RK, Hanna J, *et al.* SARS-CoV-2, SARS-CoV-1, and HIV-1 derived ssRNA sequences activate the NLRP3 inflammasome in human macrophages through a non-classical pathway. *iScience* 2021; 24: 102295.
76 Di Virgilio F, Dal Ben D, Sarti AC, *et al.* The P2X7 receptor in infection and inflammation. *Immunity* 2017; 47: 15–31.
77 Rodrigues TS, de Sá KSG, Ishimoto AY, *et al.* Inflammasomes are activated in response to SARS-CoV-2 infection and are associated with COVID-19 severity in patients. *J Exp Med* 2021; 218: e20201707.
78 Zhou Y, Fei M, Zhang G, *et al.* Blockade of the phagocytic receptor MerTK on tumor-associated macrophages enhances P2X7R-dependent STING activation by tumor-derived cGAMP. *Immunity* 2020; 52: 357–373.
79 Neufeldt CJ, Cerikan B, Cortese M, *et al.* SARS-CoV-2 infection induces a pro-inflammatory cytokine response through cGAS-STING and NF-κB. *Commun Biol* 2022; 5: 45.
80 Di Domizio J, Gulen MF, Saidoune F, *et al.* The cGAS-STING pathway drives type I IFN immunopathology in COVID-19. *Nature* 2022; 603: 145–151.

81 Pan P, Shen M, Yu Z, *et al.* SARS-CoV-2 N protein promotes NLRP3 inflammasome activation to induce hyperinflammation. *Nat Commun* 2021; 12: 4664.

82 DeDiego ML, Nieto-Torres JL, Regla-Nava JA, *et al.* Inhibition of NF-κB-mediated inflammation in severe acute respiratory syndrome coronavirus-infected mice increases survival. *J Virol* 2014; 88: 913–924.

83 Lee SM, Gai WW, Cheung TK, *et al.* Antiviral effect of a selective COX-2 inhibitor on H5N1 infection *in vitro*. *Antiviral Res* 2011; 91: 330–334.

84 Lee SM, Suk K, Lee WH. Myristoylated alanine-rich C kinase substrate (MARCKS) regulates the expression of proinflammatory cytokines in macrophages through activation of p38/JNK MAPK and NF-κB. *Cell Immunol* 2015; 296: 115–121.

85 Di Paolo NC, Shayakhmetov DM. Interleukin 1α and the inflammatory process. *Nat Immunol* 2016; 17: 906–913.

86 Cooper KM, Bennin DA, Huttenlocher A. The PCH family member proline-serine-threonine phosphatase-interacting protein 1 targets to the leukocyte uropod and regulates directed cell migration. *Mol Biol Cell* 2008; 19: 3180–3191.

87 Gally F, Kosmider B, Weaver MR, *et al.* FABP5 deficiency enhances susceptibility to H1N1 influenza A virus-induced lung inflammation. *Am J Physiol Lung Cell Mol Physiol* 2013; 305: L64–L72.

88 Mittal M, Tiruppathi C, Nepal S, *et al.* TNFα-stimulated gene-6 (TSG6) activates macrophage phenotype transition to prevent inflammatory lung injury. *Proc Natl Acad Sci USA* 2016; 113: E8151–E8158.

89 Borella R, De Biasi S, Paolini A, *et al.* Metabolic reprograming shapes neutrophil functions in severe COVID-19. *Eur J Immunol* 2022; 52: 484–502.

90 Evangelou K, Veroutis D, Paschalaki K, *et al.* Pulmonary infection by SARS-CoV-2 induces senescence accompanied by an inflammatory phenotype in severe COVID-19: possible implications for viral mutagenesis. *Eur Respir J* 2022; 60: 2102951.

91 Olivarria G, Lane TE. Evaluating the role of chemokines and chemokine receptors involved in coronavirus infection. *Expert Rev Clin Immunol* 2022; 18: 57–66.

92 Su CM, Wang L, Yoo D. Activation of NF-κB and induction of proinflammatory cytokine expressions mediated by ORF7a protein of SARS-CoV-2. *Sci Rep* 2021; 11: 13464.

93 Vora SM, Lieberman J, Wu H. Inflammasome activation at the crux of severe COVID-19. *Nat Rev Immunol* 2021; 21: 694–703.

94 Wong LR, Perlman S. Immune dysregulation and immunopathology induced by SARS-CoV-2 and related coronaviruses – are we our own worst enemy? *Nat Rev Immunol* 2022; 22: 47–56.

95 Loo J, Spittle DA, Newnham M. COVID-19, immunothrombosis and venous thromboembolism: biological mechanisms. *Thorax* 2021; 76: 412–420.

96 Perico L, Benigni A, Casiraghi F, *et al.* Immunity, endothelial injury and complement-induced coagulopathy in COVID-19. *Nat Rev Nephrol* 2021; 17: 46–64.

97 Rotoli BM, Barilli A, Visigalli R, *et al.* Endothelial cell activation by SARS-CoV-2 spike S1 protein: a crosstalk between endothelium and innate immune cells. *Biomedicines* 2021; 9: 1220.